

NASA Technical Memorandum 4783

The F/A-18 High-Angle-of-Attack Ground-to-Flight Correlation: Lessons Learned

Daniel W. Banks, David F. Fisher, Robert M. Hall,
Gary E. Erickson, Daniel G. Murri, Sue B. Grafton,
and William G. Sewall

January 1997

BOEING TECHNICAL LIBRARY
ST. LOUIS
MAILCODE: S111-1025



LM203732E

B. 113485

NASA TM-4783

NASA Technical Memorandum 4783

The F/A-18 High-Angle-of-Attack Ground-to-Flight Correlation: Lessons Learned

Daniel W. Banks and David F. Fisher
*Dryden Flight Research Center
Edwards, California*

Robert M. Hall, Gary E. Erickson, Daniel G. Murri,
Sue B. Grafton, and William G. Sewall
*NASA Langley Research Center
Hampton, Virginia*



National Aeronautics and
Space Administration
Office of Management
Scientific and Technical
Information Program

1997

TECHNICAL LIBRARY

THE F/A-18 HIGH-ANGLE-OF-ATTACK GROUND-TO-FLIGHT CORRELATION: LESSONS LEARNED

Daniel W. Banks and David F. Fisher
NASA Dryden Flight Research Center
Edwards, California

Robert M. Hall, Gary E. Erickson, Daniel G. Murri,
Sue B. Grafton, and William G. Sewall
NASA Langley Research Center
Hampton, Virginia

ABSTRACT

Detailed wind tunnel and flight investigations were performed on the F/A-18 configuration to explore the causes of many high-angle-of-attack phenomena and resulting disparities between wind tunnel and flight results at these conditions. Obtaining accurate predictions of full-scale flight aerodynamics from wind-tunnel tests is important and becomes a challenge at high-angle-of-attack conditions where large areas of vortical flow interact. The F/A-18 airplane was one of the first high-performance aircraft to have an unrestricted angle-of-attack envelope, and as such the configuration displayed many unanticipated characteristics.

Results indicate that fixing forebody crossflow transition on models can result in a more accurate match of flow fields, and thus a more accurate prediction of aerodynamic characteristics of flight at high angles of attack. The wind tunnel results show that small geometry differences, specifically nosebooms and aft-end distortion, can have a pronounced effect at high angles of attack and must be modeled in sub-scale tests in order to obtain accurate correlations with flight.

NOMENCLATURE

All force, moment, and pressure data have been reduced to coefficient form. All longitudinal data are presented in the stability axis system, while all lateral-directional data are presented in the body axis system. Moment data are referred to a moment center located at 25% of the mean aerodynamic chord.

AR	aspect ratio
b	span, ft
b'	local span, ft

C_D	drag coefficient, drag/ $q_\infty S$
C_L	lift coefficient, lift/ $q_\infty S$
$C_{L,max}$	maximum lift coefficient
C_l	rolling-moment coefficient, rolling moment/ $q_\infty S b$
C_{l_β}	lateral stability parameter or dihedral effect, $\frac{dC_l}{d\beta}$ per degree
C_m	pitching-moment coefficient, pitching moment/ $q_\infty S c$
C_n	yawing-moment coefficient, yawing moment/ $q_\infty S b$
C_{n_β}	directional stability parameter, $\frac{dC_n}{d\beta}$ per degree
C_p	pressure coefficient, $(p - p_\infty)/q_\infty$
C_Y	side-force coefficient, side force/ $q_\infty S$
\bar{c}	mean aerodynamic chord, ft
FS	full-scale fuselage station, in.
HATP	High-Angle-of-Attack Technology Program
HARV	High-Alpha Research Vehicle
LEX	leading-edge extension, or wing-body strake
LE	leading edge
M_∞	free-stream Mach number
p	surface static pressure, lb/ft ²
p_∞	free-stream static pressure, lb/ft ²
q_∞	free-stream dynamic pressure, lb/ft ²
$Re_{\bar{c}}$	Reynolds number based on mean aerodynamic chord
Re_d	Reynolds number based on forebody base diameter
S	reference area, ft ²
TE	trailing edge
y	local span distance, ft
α	angle of attack, deg

β	sideslip angle, deg
δ_f	flap deflection angle, deg
θ	circumferential angle, deg

INTRODUCTION

The design of high-performance fighter aircraft has always placed emphasis on maneuverability and agility. To this end the aerodynamic envelope of these aircraft has been expanded to include higher usable angles of attack. Significant separated and vortical flows develop over the aircraft at high angles of attack and may significantly interact. These types of flow fields result in nonlinear aerodynamics and cause significant changes in stability and control characteristics when compared with low angles of attack. The changes in stability and control at high angles of attack are difficult to predict from ground tests because of the varying sensitivities to test conditions such as Reynolds number and Mach number. It has been a goal of the NASA High-Angle-of-Attack Technology Program (HATP)¹ to develop a better understanding of these flow fields and their effect on ground-to-flight correlation.

Obtaining accurate wind-tunnel-to-flight correlation is a significant challenge. High-angle-of-attack conditions add a level of complexity to this already difficult task. In the end, a good understanding of the behavior of the associated flow fields and their potential interactions is necessary to produce useful design methodology and ground-test techniques that can accurately predict flight.

This paper reviews the results of the various wind tunnel and flight investigations of the F/A-18 configuration leading to a more comprehensive understanding of these disparities and more accurate ground-to-flight correlation at high-angle-of-attack conditions. The results reported herein were obtained from various wind tunnel tests of several 6%- and 16%-scale F/A-18 models, and flight tests of the F-18 High-Alpha Research Vehicle (HARV) conducted at the Dryden Flight Research Center, Edwards, California (DFRC).

BACKGROUND

The F/A-18 configuration, due to its interesting high-angle-of-attack characteristics, unrestricted angle-of-attack envelope, and the availability of a flight test aircraft and wind tunnel models, was adopted for much of the work of the HATP. Since the F/A-18 aircraft was one of the first aircraft capable of controlled flight at high angles of attack, it displayed many unusual characteristics that were not well understood during early high-angle-of-attack flight tests. The features of the F/A-18 aircraft that made it attractive for high-angle-of-attack research included its contoured wing-body leading-edge extensions (LEXs), and its forebody shape, which is approximately elliptical with the major axis in the vertical plane aft of the radome. The design of the F/A-18 aircraft

used the mixed flow philosophy to obtain good high-angle-of-attack characteristics without significant impact on the conventional low-angle-of-attack flight regime. At low to moderate angles of attack, the relatively low sweep wing works well. But at higher angles of attack, the leading-edge extensions (LEXs) generate strong vortices which, in addition to generating lift on the LEXs, propagate over the wings, and energize the wing flow fields, thereby extending the usable flight envelope beyond maximum lift. This same flow field is also responsible for many of the less desirable high-angle-of-attack characteristics of the F/A-18 aircraft. These strong vortices also impinge on the vertical tails and under some conditions cause severe buffeting.²⁻⁶ The forebody of the F/A-18 aircraft generates a vortex pair at high angles of attack, which interacts with the strong LEX vortices, and under some conditions can cause wing rock^{7,8} and nonlinear effects on lateral stability.

The F/A-18 development program epitomizes the challenge of ground-to-flight correlation at high-angle-of-attack conditions. Early developmental wind-tunnel tests of the F/A-18 aircraft produced inconsistent results. The most notable of these inconsistencies was between the lateral stability of large-scale models tested at relatively low Reynolds numbers and small-scale models tested at higher Reynolds numbers. The small-scale higher Reynolds number data predicted the configuration would remain laterally stable at high angles of attack, while the large-scale lower Reynolds number data indicated the configuration would become laterally unstable at angles of attack near maximum lift.⁹ Designers intuitively relied on the higher Reynolds number data as being the most representative of flight. However, early flight tests showed the lower Reynolds number data better predicted the flight characteristics at high angles of attack.

Subsequent tests of F/A-18 models and the HARV, as well as other non-F/A-18 tests have increased our understanding of high-angle-of-attack flow fields. The flow fields at these high angle-of-attack conditions typically consist of separated wakes and potentially interacting vortices. The F/A-18 high-angle-of-attack flow field is characterized by interacting forebody and LEX vortices. Since the forebody flow is more sensitive to Reynolds number effects and the LEX flow is more sensitive to Mach number effects, it is difficult to predict the high-angle-of-attack flight flow field and its interactions from sub-scale wind tunnel tests. The effectiveness of gritting to simulate higher Reynolds number boundary-layer crossflow transition at high angles of attack has been recently investigated, and has shown promising results.^{10,11} Fixing crossflow transition on the F/A-18 forebody has been shown to reduce differences between wind tunnel and flight aerodynamic results.^{12,13} The effects of small geometric differences, such as airdata probes and deformations for wind-tunnel supports, can have a pronounced effect at high angles of attack and are responsible for some of the differences seen between F/A-18 aircraft and model tests.

MODELS, FACILITIES, AND INSTRUMENTATION

The data presented in this paper were obtained from multiple wind-tunnel entries with several F/A-18 6%- and 16%-scale models and flight tests that were conducted with the HARV. The ground and flight tests were coordinated as well as possible to obtain meaningful comparisons between ground and flight data. This coordination included a common set of measurements, and flight conditions (α , β , and M_∞) closely matched to the wind tunnel conditions. Also, for model

data, all leading- and trailing-edge flap positions were made consistent with the flight vehicle configuration at that flight condition. The configuration that was tested on the HARV at $\alpha \geq 26^\circ$ and $M_\infty \leq 0.76$ was $\delta_{LE} = 33^\circ$ and $\delta_{TE} = 0^\circ$.

6% Models

There were two 6% model configurations that are reported herein. The first is referred to as the MD/Navy 6% model (fig. 1). This model is the 6% wind-tunnel model originally used by McDonnell Douglas (St. Louis, Missouri) and the U.S. Navy during the design and test of the F/A-18, which was tested in the current F/A-18 configuration. The second 6% model consisted of the back end of the MD/Navy 6% model with a more recently constructed and instrumented forebody section (from nose apex back to LEX/wing juncture). This forebody had pressure ports from the nose back to the mid LEX region and is referred to as the NASA 6% model (fig. 2). Thus, these two models/configurations shared the same wings, empennage, and support system hardware. The pressure instrumentation consisted of 440 pressure orifices distributed circumferentially at 5 stations on the nose and spanwise at 3 stations across the LEXs, as shown in figure 3. The pressures were measured by internally mounted electronic scanning pressure modules located within the forebody. The on-surface flow visualizations were obtained with a mixture of titanium dioxide (TiO_2), mineral oil, and a small amount of oleic acid added for dispersion.¹⁴ The mixture was applied to the model, the tunnel was then brought on condition long enough for the mixture to set, and then rapidly brought to a static condition when photographic documentation was taken. The off-surface flow visualizations were obtained with water vapor (injected or natural) and a laser light sheet in the wind tunnel, this was recorded with video cameras.¹⁵ The 6% model wind-tunnel



Figure 1. MD/Navy 6% F/A-18 model in the NASA Langley 7- x 10-ft High Speed Tunnel.

tests were conducted in NASA Langley Research Center's 14- × 22-ft Subsonic Tunnel, 7- × 10-ft High Speed Tunnel, Low-Turbulence Pressure Tunnel, and in the David Taylor Research Center's 7- × 10-ft Transonic Wind Tunnel.

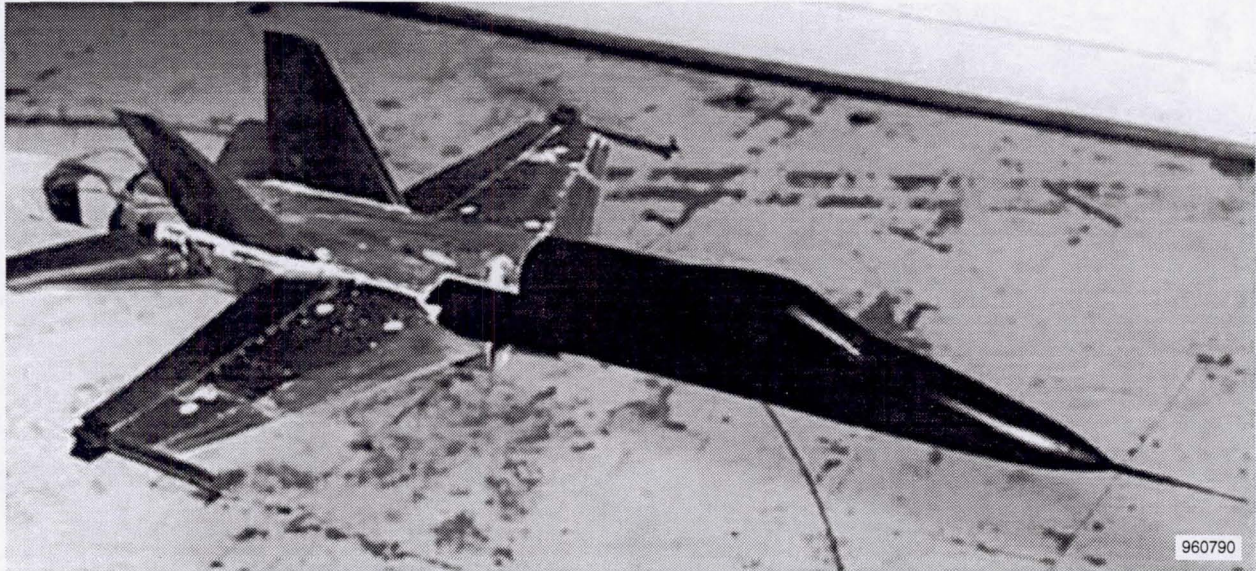


Figure 2. NASA 6% F/A-18 model in the NASA Langley 14- × 22-ft Subsonic Tunnel.

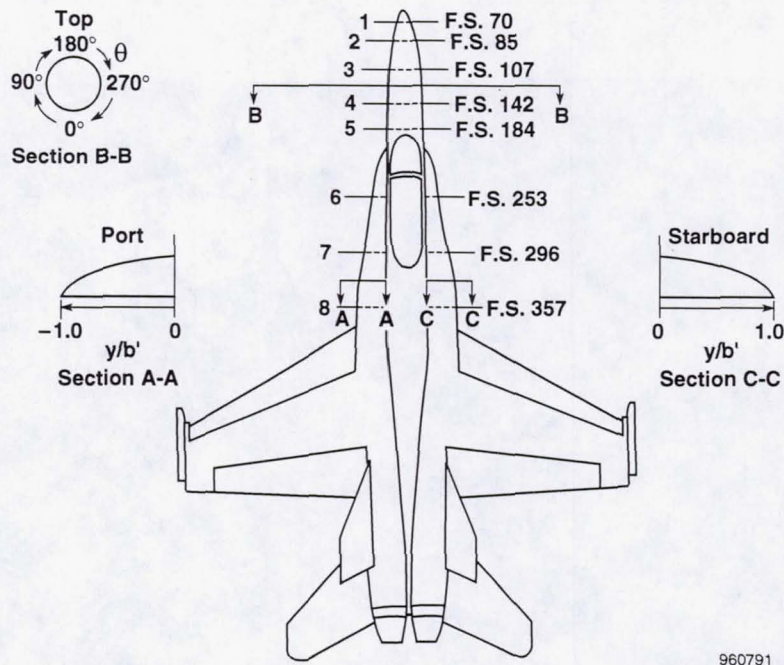


Figure 3. Pressure measurement locations on F/A-18 forebody and LEX.

16% Models

There are two 16% low Reynolds number models reported herein. The first was modified from an older preproduction 16%-scale F/A-18 model configuration and although it was modified to more closely represent the F/A-18 configuration as it evolved, still incorporated some differences. Figure 4 shows this model and is called the NASA-1 16% F/A-18 model. There are limited flow visualization results presented here from this model. The second 16%-scale F/A-18 model represents the current F/A-18C configuration and was of much higher fidelity than the NASA-1 16%-scale model. This second F/A-18 model is referred to as the NASA-2 16% model and shown in figure 5. The NASA-2 16% model was also designed with more instrumentation than the NASA-1 16% model and all of the 6% models. Both 16% models were constructed of lightweight fiberglass since they were also used as free-flight models and therefore were limited to lower dynamic pressure than the 6% models. The NASA-2 16% model also included removable components; some that were instrumented to determine the flow field effects of having pressure port roughness effects, and others to assess changes in geometry (e.g. the noseboom). The results from the NASA-2 16% model will be used for all quantitative data (force, moment, and pressure distributions) since it had a higher degree of fidelity in both geometry and data, and because of its flexibility in replaceable components. The NASA-2 16% model had a more extensive number of surface pressure measurements than the instrumented NASA 6% model; however, only those which correspond to the fuselage stations of the NASA 6% model will be reported here (fig. 3). Both of the 16% wind tunnel models were tested in NASA Langley Research Center's 14- × 22-ft Subsonic Tunnel and 30- × 60-ft Tunnel. The on-surface flow visualization was obtained from tests of the NASA-1 16% model. The technique was essentially the same as described for the 6% model, with the exception of the mixture being thinner to accommodate the lower dynamic pressures.

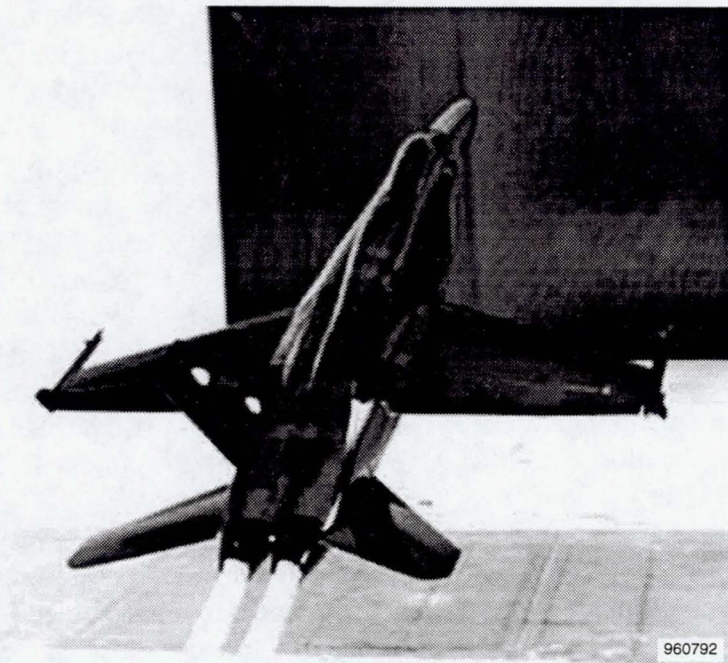


Figure 4. NASA-1 16% F/A-18 model in the NASA Langley 14- × 22-ft Subsonic Tunnel.

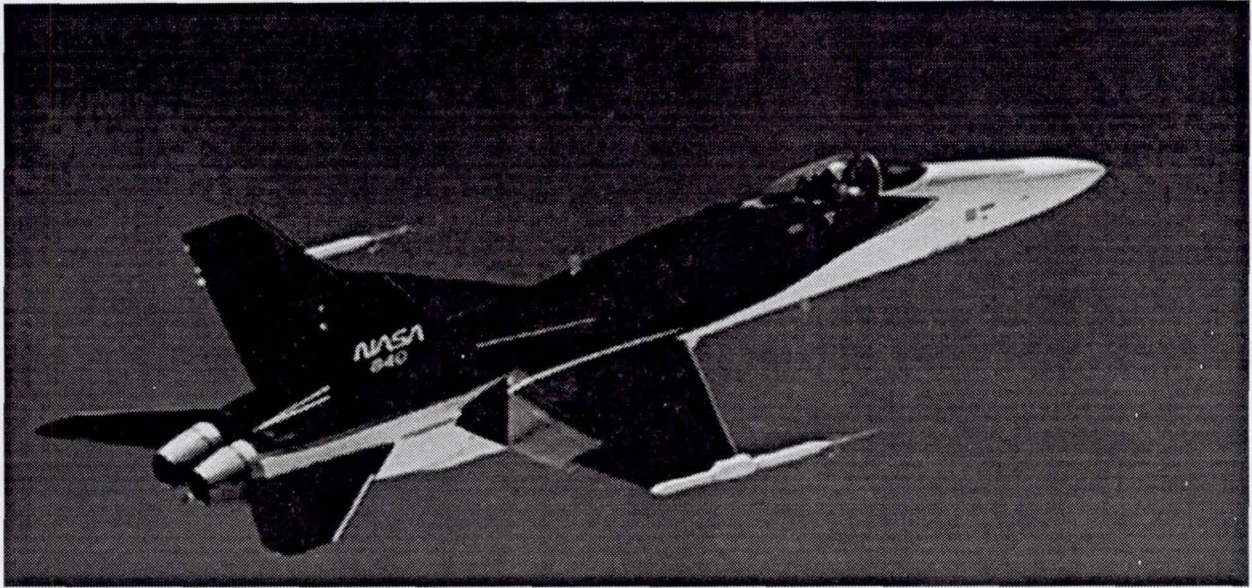


Figure 5. NASA-2 16% F/A-18 model in the NASA Langley 30- × 60-ft Tunnel.

HARV Flight Tests

Dedicated flight tests were conducted with the F-18 HARV at the NASA Dryden Flight Research Center, Edwards, California (fig. 6). Although the vehicle was heavily modified for various phases of the program,^{16,17} the data shown in this report apply to the basic F/A-18 configuration. Some data were obtained with and some without the LEX fences that are part of the current F/A-18 configuration. The F/A-18 HARV has both leading- and trailing-edge flaps that are scheduled with angle of attack and Mach number. At $\alpha \geq 26^\circ$ and $M \leq 0.76$ the leading-edge flaps are deflected to their maximum of 33° and the trailing-edge flaps are set to 0° . The HARV was flown in the F/A-18 fighter-escort configuration, without stores, and the wingtip missile rails were modified to carry special camera pods and wingtip airdata probes. Also the HARV was tested predominantly without LEX fences installed. The HARV was instrumented with surface pressure ports¹⁸ at the same fuselage stations as shown in figure 3 for the 6% model. On-surface flow visualization was obtained in flight with a mixture of an evaporating fluid and dye.¹⁹ The fluid and dye mixture was pumped out of the ports, which were later used for pressure measurements. The dye patterns set quickly as the fluid evaporated and were preserved until postflight photos could be obtained. Off-surface flow visualization was obtained in flight with injected smoke at the apex of the LEX's and nose.^{20,21}

Except where noted, all data presented was obtained from configurations without nosebooms or LEX fences. Also, except where noted, all wind tunnel data was obtained from models with only the nosering grit pattern used for low-angle-of-attack forebody transition fixing, but not the twin strips grit pattern used for high-angle-of-attack forebody crossflow transition.



EC 88 0095-002

Figure 6. NASA HARV in flight at the NASA Dryden Flight Research Center, Edwards, California.

RESULTS AND DISCUSSION

Basic Aerodynamics

The basic longitudinal aerodynamic characteristics of the F/A-18 in the high-angle-of-attack configurations from wind tunnel tests are shown in figure 7. The longitudinal characteristics are similar between the models, with the major differences being small changes in $C_{L,max}$ and variations in pitching moment. Maximum lift occurs at approximately $\alpha = 40^\circ$, with $C_{L,max} \sim 1.80$. The NASA 6% model has greater pitch stability than the NASA-2 16% model at angles of attack from 25° to 40° , and greater nose down pitching moment from $\alpha = 10^\circ$ to $\alpha = 45^\circ$. Some effects of model geometry on this pitching moment difference will be discussed later in this report.

The lateral-directional characteristics of the NASA 6% and NASA-2 16% models in the high-angle-of-attack configuration at $\alpha = 40^\circ$, are shown in figure 8. An angle of attack of 40° is of significant interest since this is the angle of attack for maximum lift. The NASA 6% model shows higher levels of lateral stability than the NASA-2 16% model at this angle of attack ($-4^\circ \leq \beta \leq 4^\circ$). The effects of Reynolds number, grit, and noseboom on lateral stability will be discussed later in the report.

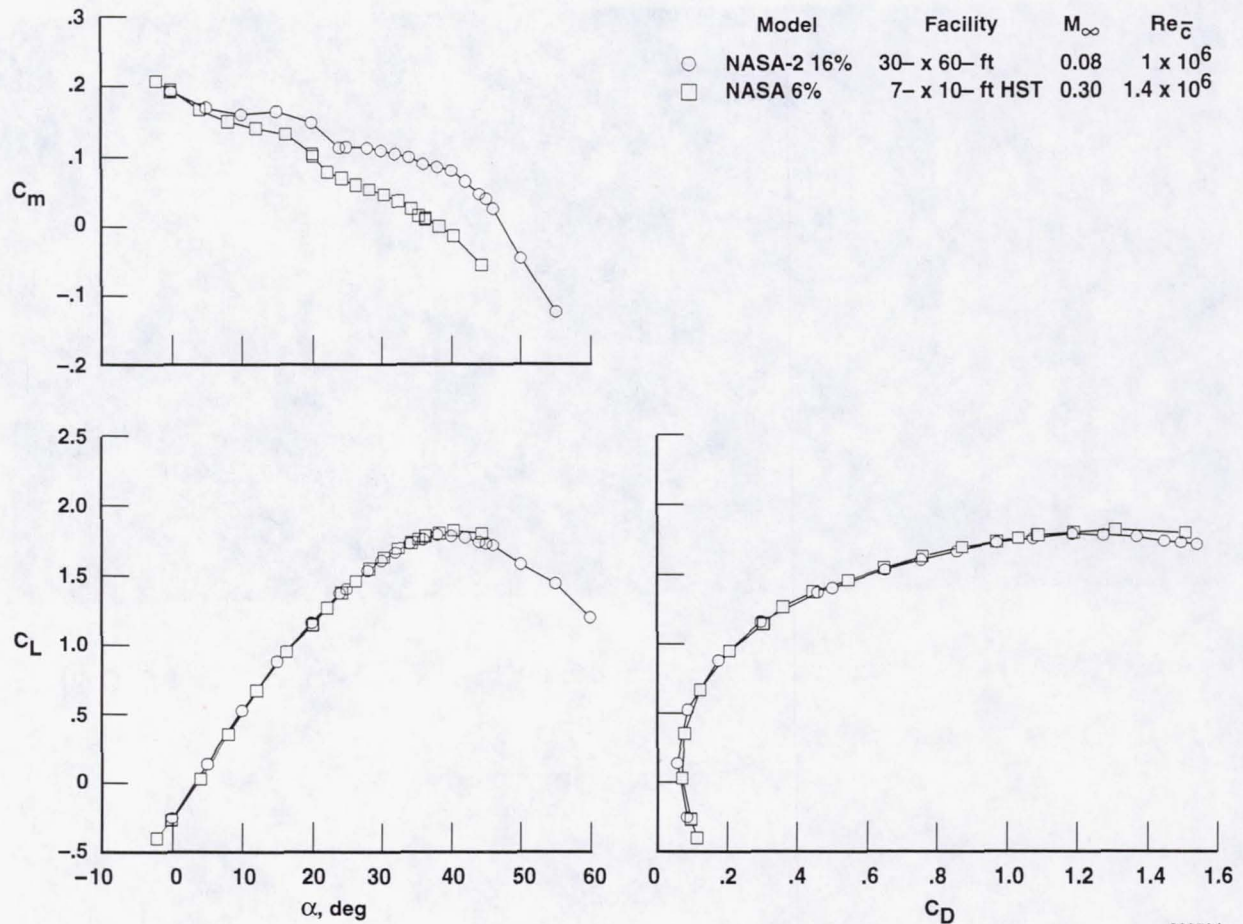
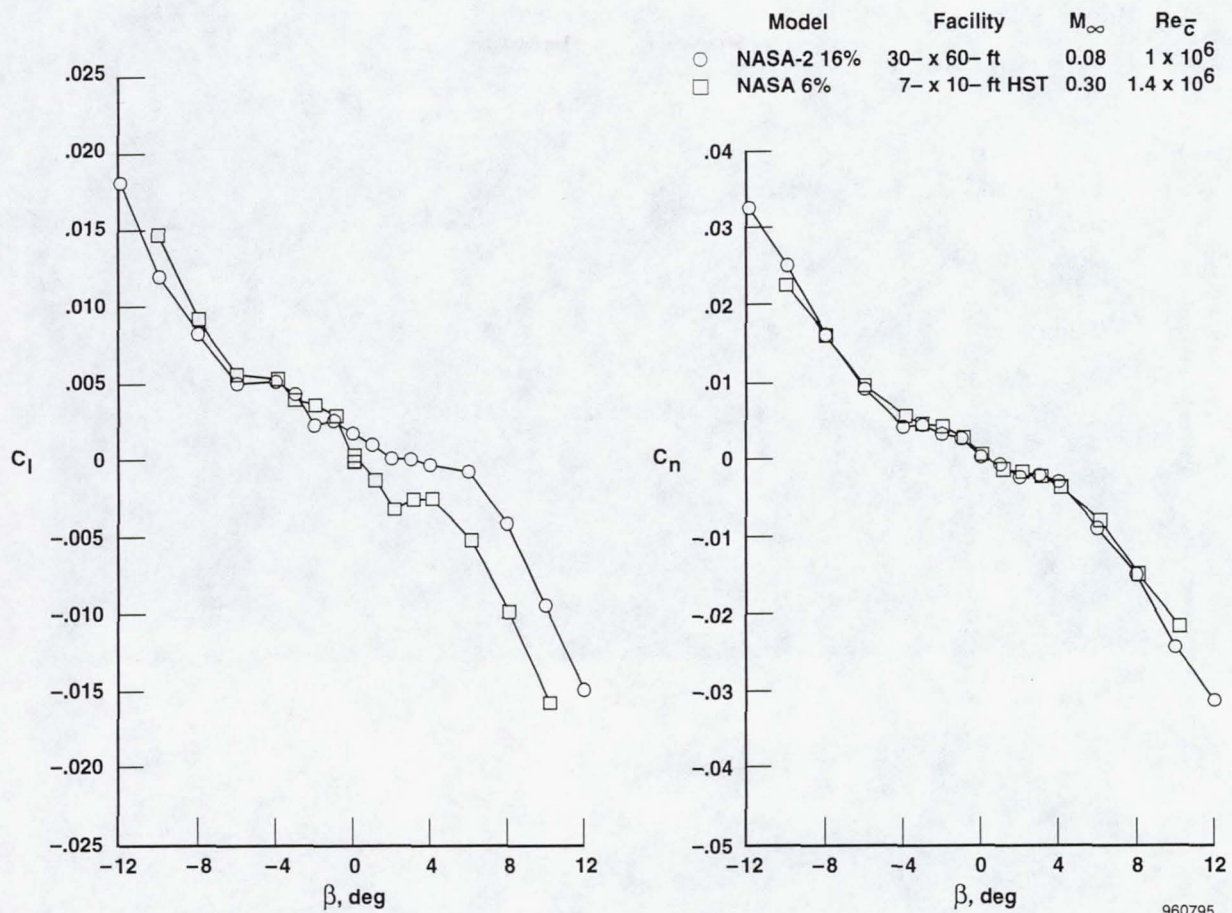


Figure 7. Longitudinal aerodynamics of F/A-18 models. $\beta = 0^\circ$, $\delta_{fLE} = 33^\circ$, $\delta_{fTE} = 0^\circ$, $\delta_{HT} = -12^\circ$.

The on-surface flow characteristics of the NASA-1 16% model at $\alpha = 36^\circ$ and MD/Navy 6% models at $\alpha = 35^\circ$ (both at $Re_{\bar{c}} \sim 1$ million) are shown in the oil flow visualization of figures 9 and 10 respectively. While the two models were tested at nearly the same Reynolds number and angle of attack the forebody flow field visualizations show some significant differences. The most notable features on the NASA-1 16% model are a void region, seen in black, extending approximately from just behind the nose apex aft to the LEX juncture. This feature is most likely a laminar separation bubble, which would indicate that the flow upstream of it is laminar. On the front half of the nose the void is terminated by streamlines in an opposing direction. These lines indicate that the flow has separated aft of the bubble in this region (most likely laminar separation). On the rear half of the nose the void region is terminated by an almond-shaped region where the streamlines are in the same general direction as prior to the bubble. This evidence indicates a turbulent reattachment in this region. The streamlines in this almond-shaped region show a difference in the texture, appearance of higher surface shear can be noticed, a further indication that the flow in this small region is turbulent. On the leeward side of the model additional voided regions are noticed which appear to be caused by the impingement of the secondary separation vortex. These voided regions propagate over the canopy. A similar feature is seen near the leading edge of the LEX. Overall, the nature of the flow field of the NASA-1 16% model forebody is transitional, mostly laminar with small areas of turbulent flow.



960795

Figure 8. Lateral-directional aerodynamics of F/A-18 models. $\alpha = 40^\circ$, $\delta_{fLE} = 33^\circ$, $\delta_{fTE} = 0^\circ$, $\delta_{HT} = -12^\circ$.

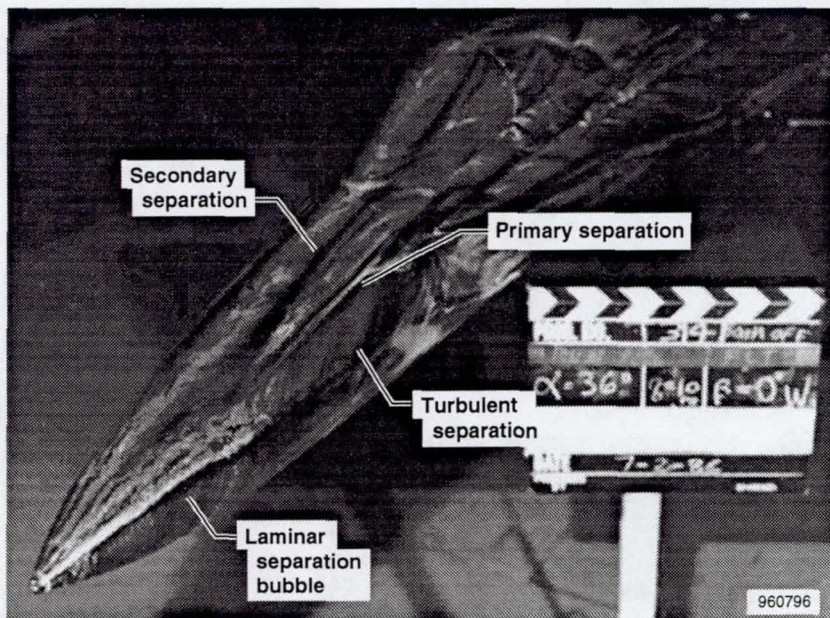


Figure 9. Forebody oil flow visualization of NASA-2 16% F/A-18 model. $\alpha = 36^\circ$, $M_\infty = 0.08$, $Re_{\bar{c}} \sim 1 \times 10^6$.

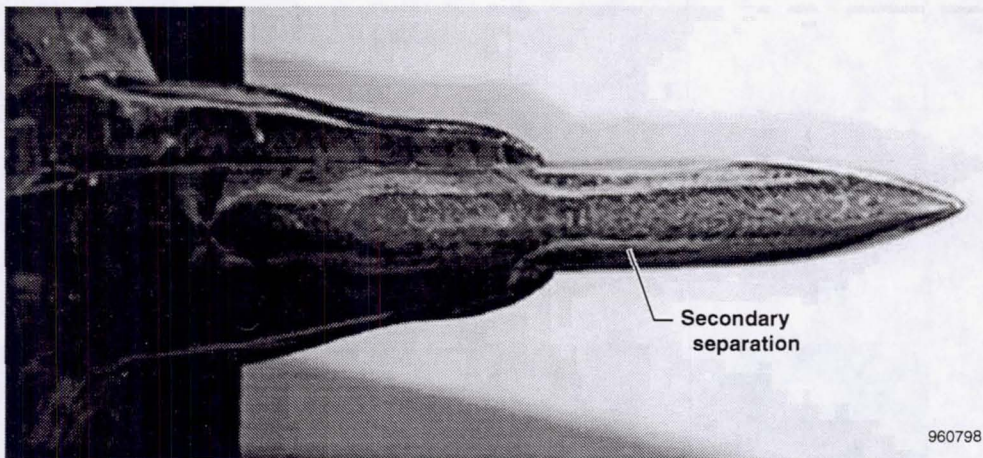
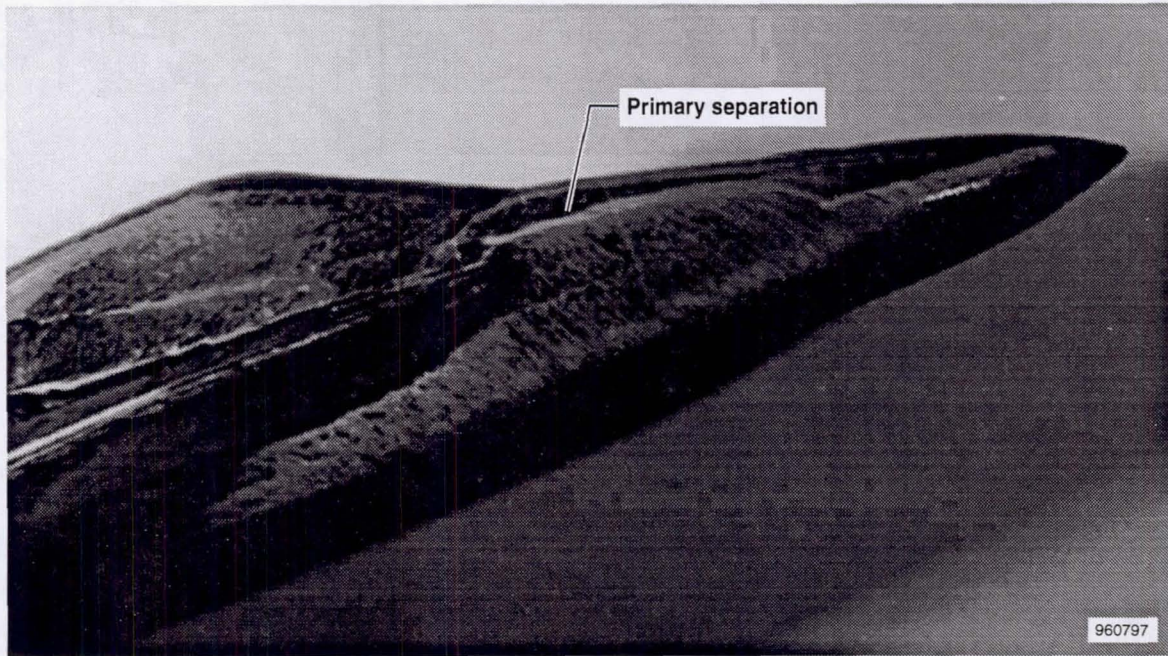


Figure 10. Forebody oil flow visualization of NASA 6% F/A-18 model: two views $\alpha = 36^\circ$, $M_\infty = 0.22$, $Re_{\bar{c}} \sim 1 \times 10^6$.

The surface flow of the MD/Navy 6% model, shown in figure 10, indicates some distinct differences from that of the NASA-1 16% model, even though they were tested at nearly the same Reynolds number and angle of attack. This model does not show any of the laminar separation bubbles that were prominent on the NASA-1 16% model. The MD/Navy 6% model does show a pooling near the 90° and 270° positions close to $2/3$ the length of the nose, which would indicate laminar separation. Aft of this the flow appears to remain attached. There are no voided regions on the leeward side. There is a demarcation which is most likely caused by secondary separation, but is significantly weaker than that seen with the NASA-1 16% model and terminates at the LEX apex. Overall, the MD/Navy 6% model also appears to be transitional but with different features than that of the NASA-1 16% model. Some of these differences can be attributed to differences in

dynamic pressure and to the viscosity effects of the oil on changing the local geometry. The MD/Navy 6% model was tested at a higher dynamic pressure and thus the oil mixture was somewhat more viscous, so the smaller model would also be more prone to local variations in geometry from the oil. The extent of transitional flow on the MD/Navy 6% forebody was more difficult to determine than the NASA-1 16% because of effects of the oil on the MD/Navy 6% model and the resultant patterns. However, it appears that the flow field present (extent of transitional flow) on the forebody of each model was different even though this visualization was obtained at nearly the same Reynolds number.

On-surface flow characteristics of the HARV at $\alpha = 34^\circ$, and $M_\infty = 0.3$ are shown in figure 11. The HARV displays a similar surface topology to that of the models with some notable differences. The forebody flow of the HARV appears to be fully turbulent aft of the radome. There is a small run of laminar flow on the radome, but it has fully transitioned by FS 107.⁸ Recall that the NASA-1 16% model showed a significant vortex structure pass over the canopy and the MD/Navy 6%, under some conditions, showed a similar although less defined vortex which did not propagate over the canopy. Although the HARV had no flow visualization on the canopy the secondary separation lines are well defined up to the canopy.

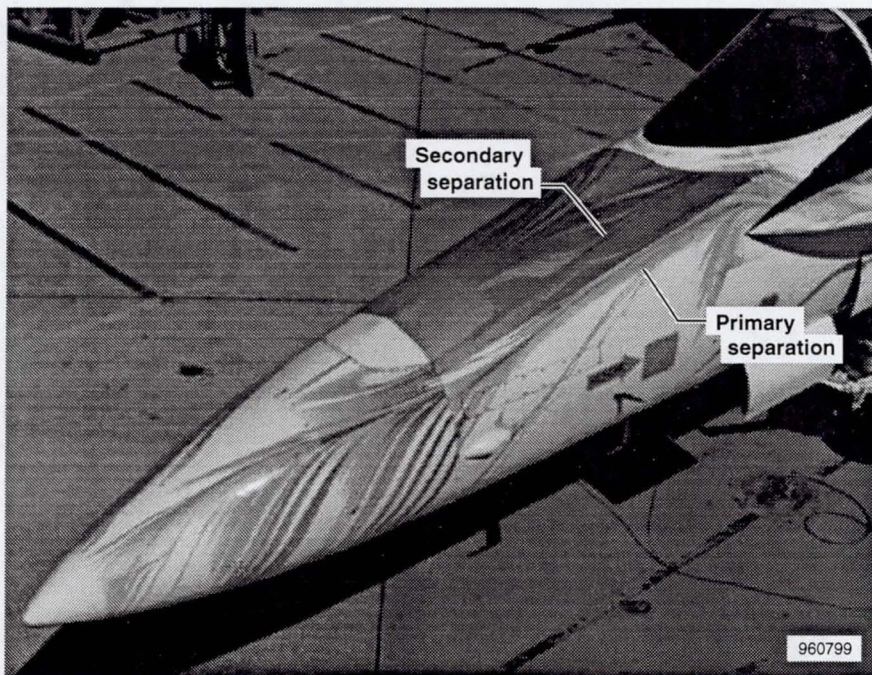


Figure 11. Forebody flow visualization of NASA HARV. $\alpha = 34^\circ$, $M_\infty = 0.3$, $Re_{\bar{c}} \sim 8.5 \times 10^6$.

The off-surface flow visualization of the HARV at $\alpha = 39^\circ$, and $M_\infty = 0.24$ is shown in figure 12. This flow visualization was obtained with smoke injection into the feeding sheet of the forebody vortex and natural condensation in the LEX vortex. The off-surface visualization (fig. 12) shows the vortices propagating over the canopy and interacting with the LEX vortex. It is presumed that this type of interaction is also present on the models at some conditions, but it appears not to be present at many of the conditions tested.

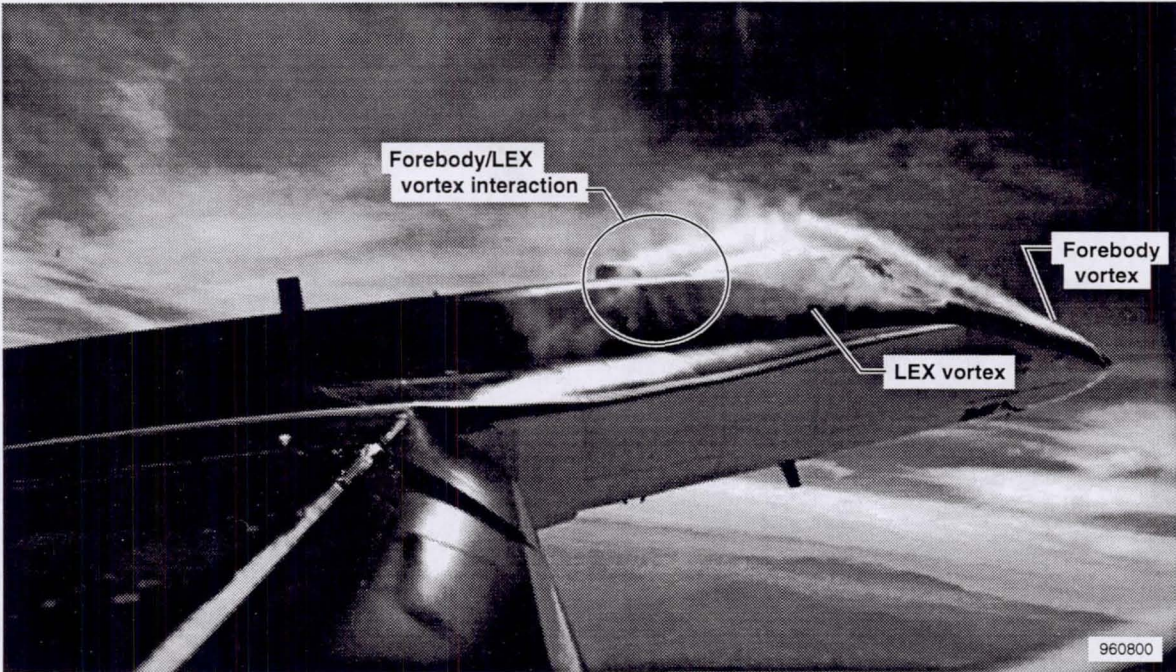


Figure 12. Off-surface smoke flow visualization of NASA HARV. $\alpha = 39^\circ$, $M_\infty = 0.24$, $Re_{\bar{c}} \sim 9.7 \times 10^6$.

The forebody surface pressure distributions of the two models and the HARV at $\alpha = 40^\circ$ are shown in figure 13. The areas of most interest are the forebody suction peaks (vortex footprint). These suction peaks indicate the presence of strong forebody vortices close to the surface, which generate high surface velocities and low pressures. These are evident at $\alpha = 40^\circ$ station 142. The flight data also shows a faster pressure recovery than the models ($75^\circ \leq \theta \leq 135^\circ$ and $225^\circ \leq \theta \leq 255^\circ$ at FS 142). The wind-tunnel model data do not show these strong suction peaks (vortex footprint), but otherwise match the HARV data quite well. The character of the flight and wind tunnel forebody vortex suction peaks correlates well with what was seen in the flow visualizations; that is, the models at these conditions showed less vortical influence near the leeward plane of symmetry when compared with the HARV.

While the wind tunnel model forebody pressure data matched flight well everywhere except for the forebody vortex suction peaks, the models did not correctly predict the full-scale flight lateral-directional behavior at $\alpha = 40^\circ$ (maximum lift). *This strongly implies that the forebody flow field contributes to this disparity in lateral stability.* This forebody flow characteristic is consistent with the behavior seen on ogive cylinders at high angles of attack, which is strong vortex development at laminar and fully turbulent conditions and significantly less at transitional conditions.²²⁻²⁴ This implies that correct boundary-layer simulation on wind tunnel models is important to accurate prediction of airplane lateral-directional stability characteristics.

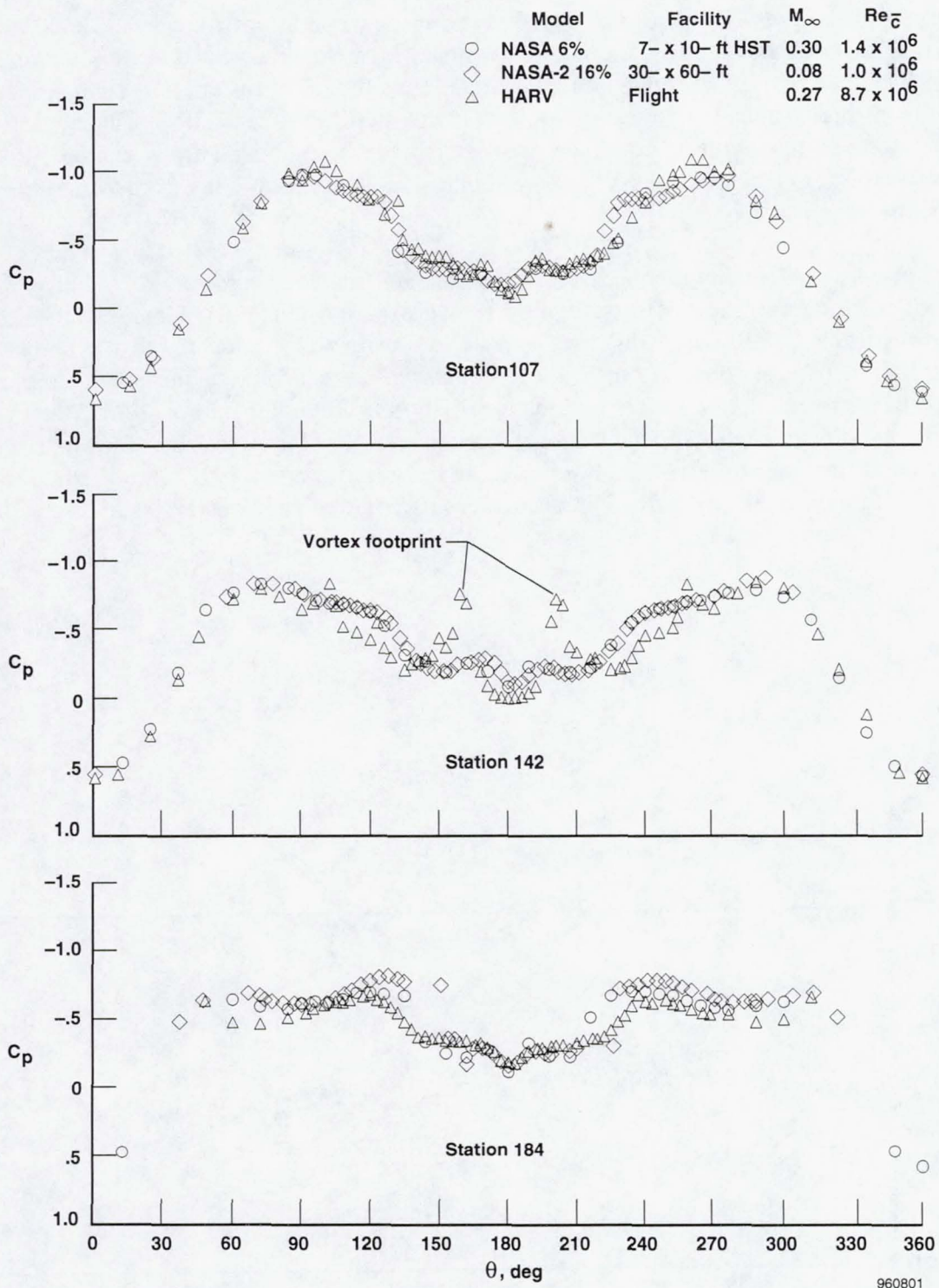


Figure 13. Forebody surface pressure distribution of F/A-18 models and HARV. $\alpha = 40^\circ$.

Mach Effects

Effects of compressibility become apparent at transonic conditions when local shock waves develop. These shock waves cause premature boundary-layer separation and vortex bursting,²⁵ and change the nature of the highly interactive separated flow field. The result is seen in nonlinear aerodynamics at high angles of attack. However, where significant local flow acceleration occurs effects can be seen at significantly lower free-stream Mach numbers. Highly cambered or swept surfaces with sharp leading edges (e.g. strakes and LEXs) may show some compressibility effects even below $M_\infty = 0.3$.

The effects of Mach number on lateral-directional characteristics for the MD/Navy 6% model is shown in figure 14. These effects are only shown for the MD/Navy 6% model, since the 16% model was limited to low dynamic pressures. These tests were conducted at the David Taylor Research Center 7- x 10-ft Transonic Tunnel, which runs at reduced total pressure at higher Mach numbers. This reduced, but did not eliminate, variation in Reynolds number with Mach number. There are significant changes in the lateral-directional stability for increasing Mach numbers. Figure 14 shows the basic trend, which is an increase in lateral stability and a decrease in directional stability with increasing Mach number and increasing angle of attack at angles of attack $\alpha > 30^\circ$

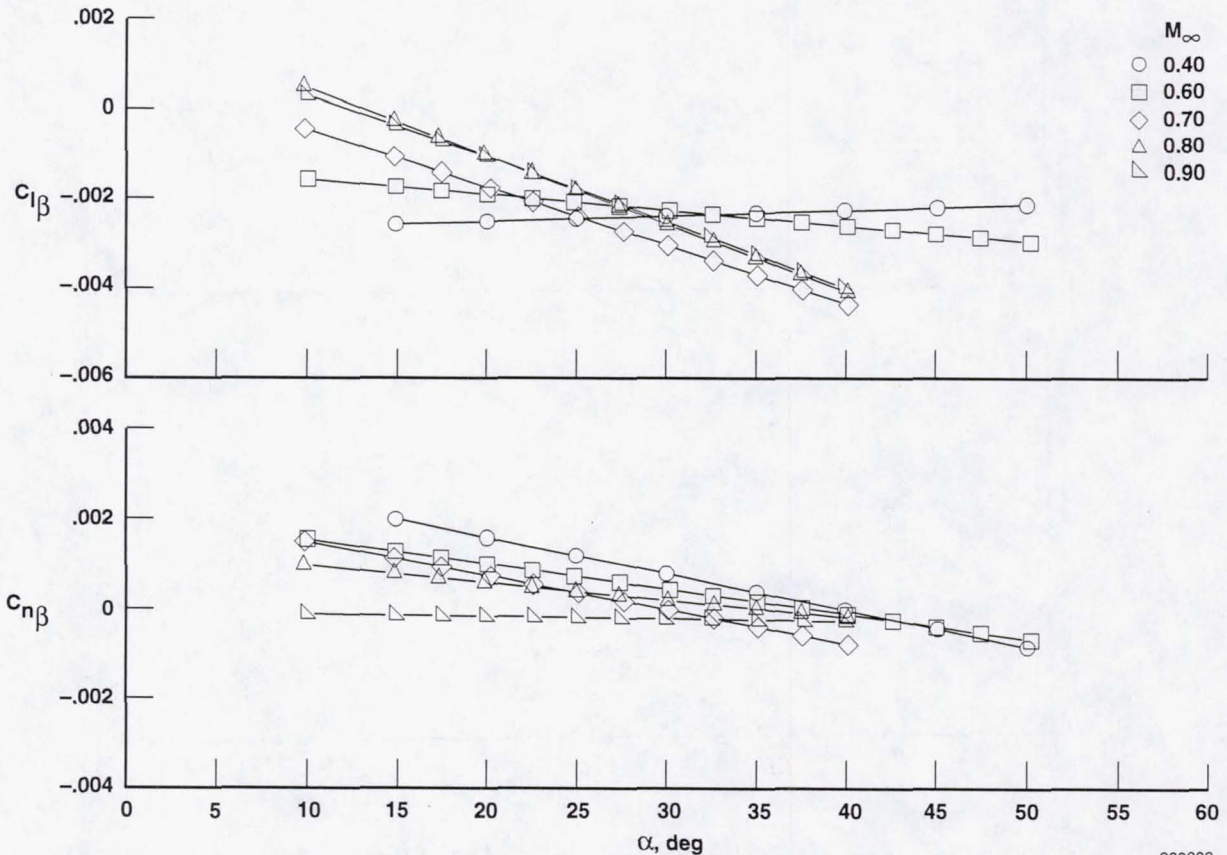


Figure 14. Effects of Mach number on lateral-directional stability of NASA 6% F/A-18 models. $\delta_{fLE} = 33^\circ$, $\delta_{fTE} = 0^\circ$, $0^\circ \leq \beta \leq 4^\circ$.

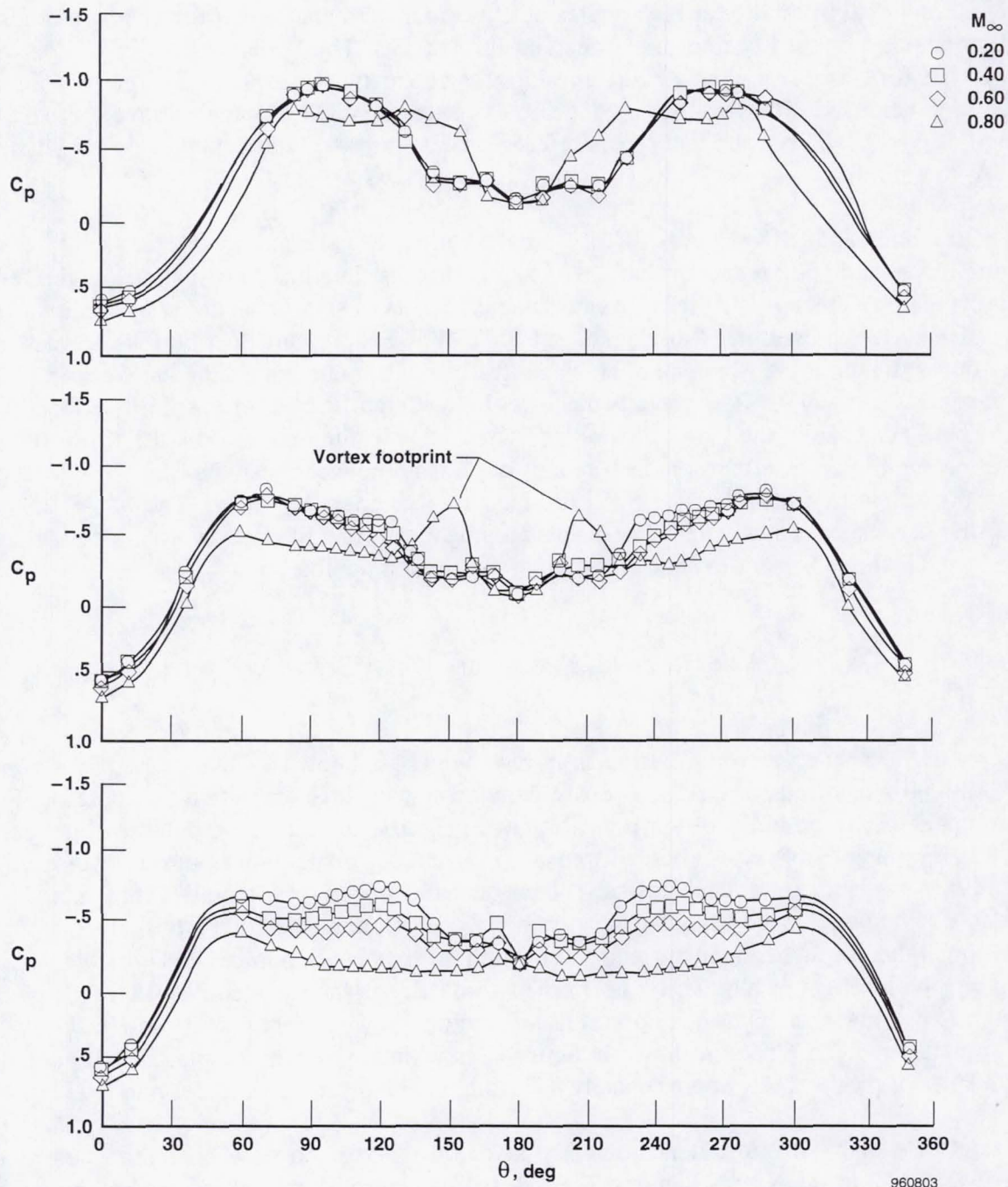
and $M_\infty < 0.9$. At $M_\infty = 0.9$ there is no change in lateral stability from $M_\infty = 0.8$ and directional stability increases slightly for increasing angles of attack. At high angles of attack C_{l_β} is a stronger influence on departure resistance than is C_{n_β} , and it is typical for fighter-type configurations to have directional instability at high angles of attack. Gradual changes at lower Mach numbers are likely caused by locally transonic effects in the vortices. The large changes in C_{l_β} between $M_\infty = 0.6$ and $M_\infty = 0.7$ are most likely a result of the formation of local shocks on the wing and LEXs. In general the MD/Navy 6% model displays laterally stable behavior above $\alpha = 10^\circ$ and through $M_\infty = 0.9$. This trend had typically been observed throughout the early development of the F/A-18 aircraft.

The forebody and LEX pressure distributions at various Mach numbers at $\alpha = 40^\circ$ are shown in figures 15(a) and 15(b) respectively. The LEX pressure distributions were obtained in the David Taylor Research Center 7- \times 10-ft Transonic Tunnel. There is a significant effect of Mach number on the LEX surface pressure distributions (fig. 15(b)). The LEX pressure distributions decrease and flatten out with increasing Mach number. The effects of Mach number on the LEX pressures are seen to persist below $M_\infty = 0.3$, typically the lower limit of significant compressibility effects. This is most likely caused by the high accelerations around the leading edge of the LEX resulting in local transonic flow. The effects on the forebody are less pronounced than the LEX. The forebody surface pressures are relatively insensitive to Mach number up to $M_\infty = 0.6$. The $M_\infty = 0.8$ data shows the suction peaks associated with the development of strong forebody vortices. This change at $M_\infty = 0.8$ is likely a result of shock induced separation on the forebody.

Effect of Reynolds Number and Forced Transition

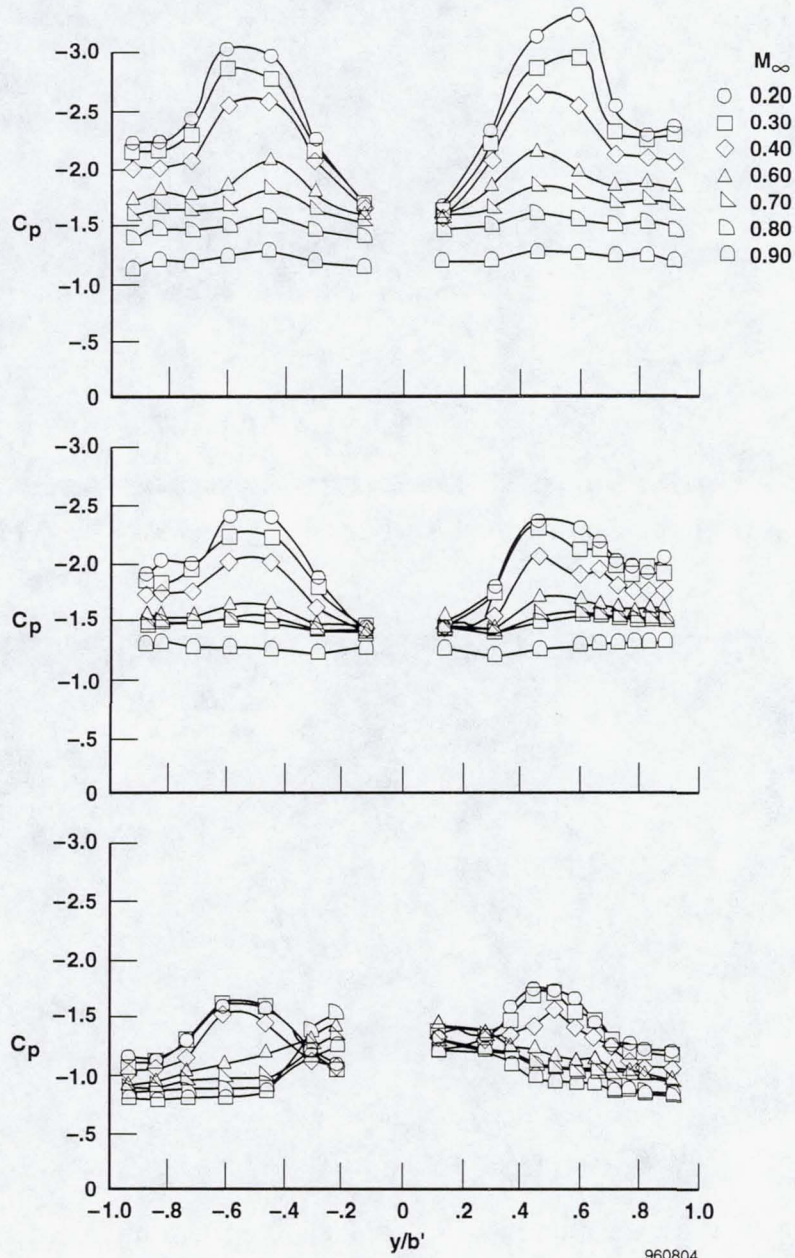
Reynolds number effects on lifting surfaces have long been known to have a significant impact on model-to-flight correlations. As previously shown boundary-layer transition and therefore Reynolds number effects on forebody surfaces also have a significant effect on ground-to-flight correlations at high angles of attack. Forced transition techniques analogous to those developed for attached flows on wings and other surfaces²⁶ have been developed for forebodies at high angles of attack in conventional wind tunnels.¹⁰ By properly transitioning the forebody boundary layer, simulating higher Reynolds numbers, and testing at the correct Mach number it is possible to more accurately predict flight results. The grit pattern that was used in the reported F/A-18 tests included a standard nosering, which has been used for conventional low/moderate angle-of-attack testing, and a so-called twin strip pattern shown in figure 16 in which two strips are placed longitudinally on both sides of the forebody approximately 54° from the windward attachment line.

The effects of a fully turbulent boundary layer on the surface flow characteristics of the NASA 6% model in the NASA Langley 7- \times 10-ft High Speed Tunnel were assessed by adding additional TiO_2 particulates (to increase roughness) and testing at a higher dynamic pressure. The result is shown in figure 17 at $\alpha = 35^\circ$ and $M_\infty = 0.5$, and many differences can be seen from that seen in figure 10. Recall figure 10 ($Re_c = 1 \times 10^6$, $M_\infty = 0.22$) which showed very weak structure on the lee side of the forebody, the structures terminated at the LEX apex and did not pass over the canopy. Figure 17 now shows the strong vortex features on the forebody propagating over the canopy at $\alpha = 35^\circ$ and $M_\infty = 0.5$ ($Re_d = 600,000$). Also the previously seen pooling and wedges



(a) Forebody.

Figure 15. Effect of Mach number on surface pressure distributions of NASA 6% F/A-18 model. $\alpha = 40^\circ$.



(b) LEX, upper surface.

Figure 15. Concluded.

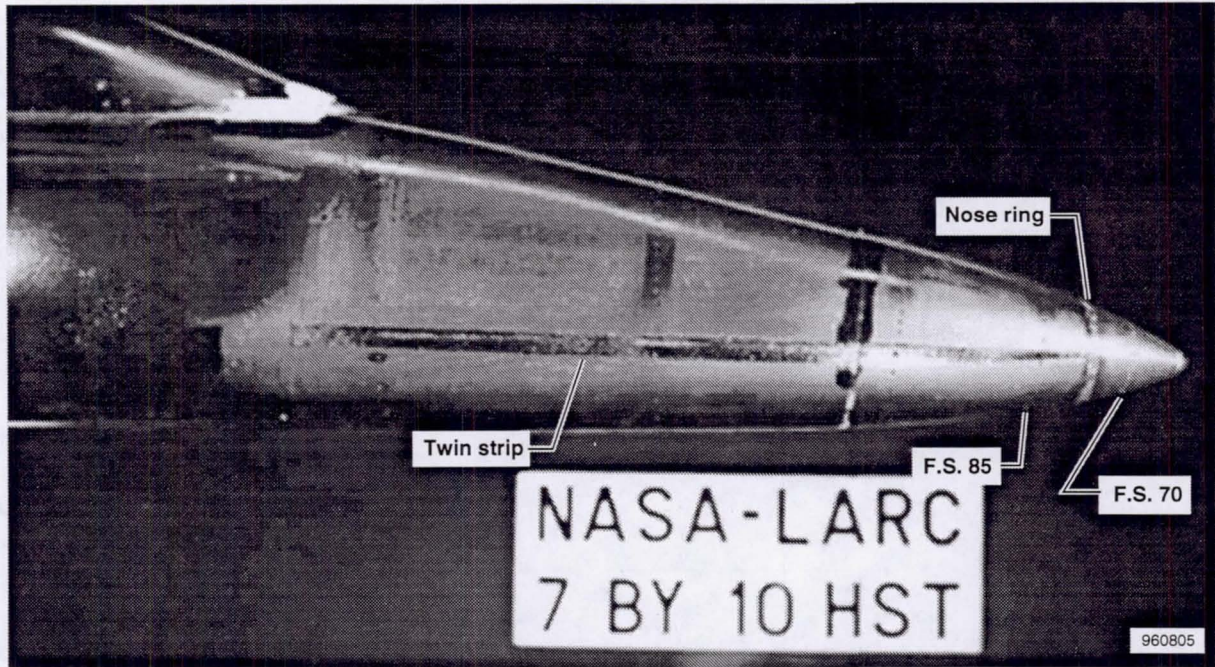


Figure 16. Photograph of twin strip forebody transition grit on NASA 6% F/A-18 model.

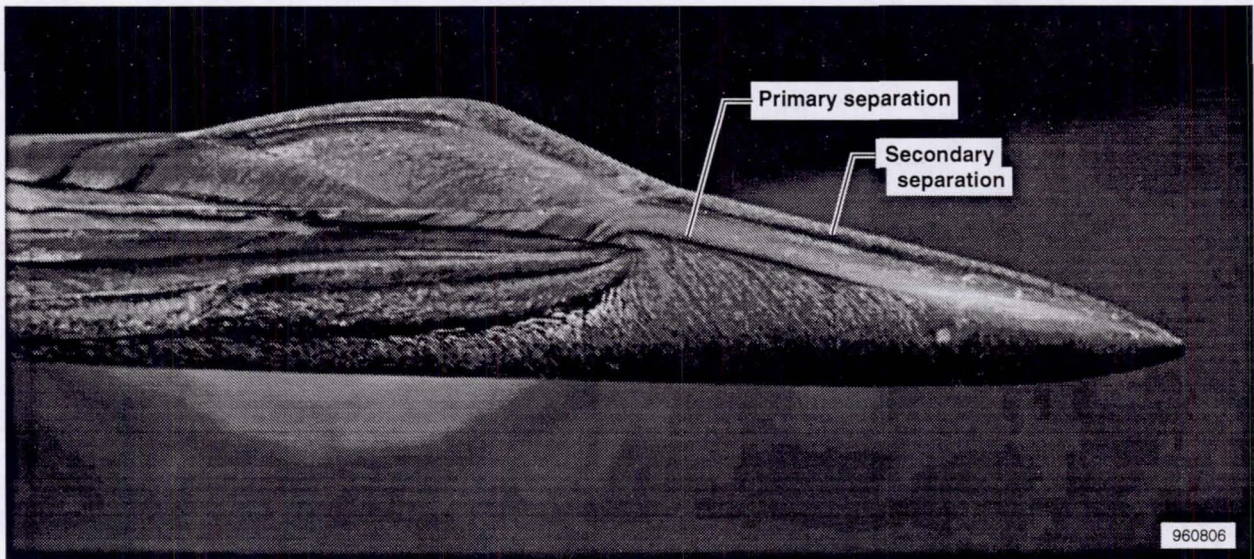


Figure 17. Forebody flow visualization of NASA 6% F/A-18 model with forced transition. $\alpha = 35^\circ$, $M_\infty = 0.5$, $Re_{\bar{c}} \sim 2.1 \times 10^6$.

are no longer present and the separation lines are much more defined, an indication that they were likely generated by much higher surface shear and stronger vortical flow. This difference in flow visualization shows the local flow differences with a change in free-stream condition and boundary layer state.

At high angles of attack the local surface flow has a significant component in the cross-flow direction. Therefore, the twin strips are placed so that they transition each of the streamlines as they move around the body. Figure 18 shows the surface pressure distribution at fuselage stations 107, 142, and 184 with and without this fixed cross-flow transition at $\alpha = 36.4^\circ$ and $M_\infty = 0.30$. The comparison shows that the major effect is the much more evident vortex footprints (suction peaks

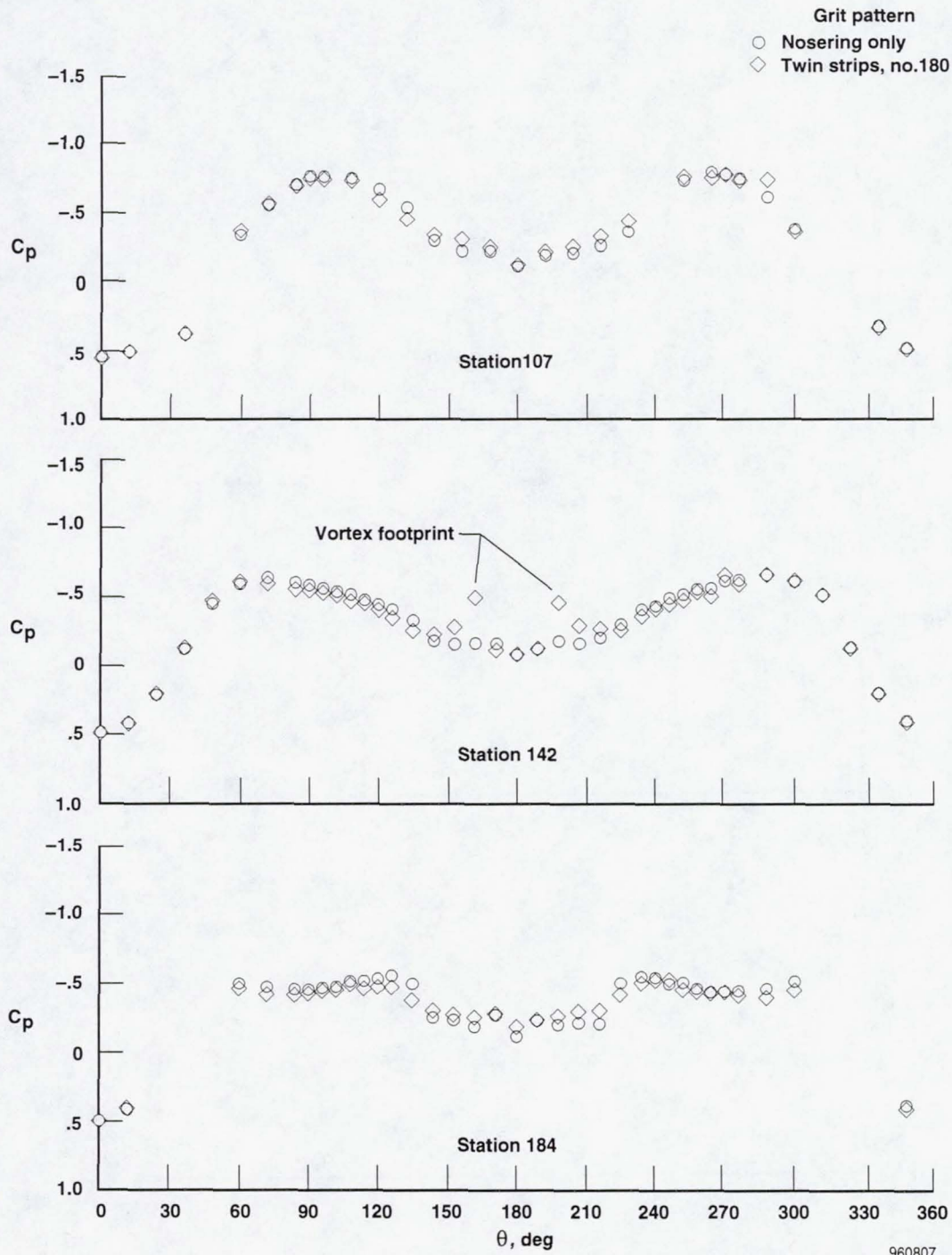


Figure 18. Effect of fixed transition on forebody pressure distribution of NASA 6% F/A-18 model. $\alpha = 36.4^\circ$, $M_\infty = 0.3$, $Re_{\bar{c}} \sim 1.4 \times 10^6$.

at FS 142) on the leeward side when the crossflow is tripped. This, again, is evidence of the strength of the forebody vortices, which are attenuated at transitional conditions.^{22,24} A comparison of the 6% model test at $\alpha = 40^\circ$ and $M_\infty = 0.30$ with fixed cross-flow transition to the HARV is shown in figure 19. This shows a well-matched surface pressure distribution, with the forebody suction peaks just slightly lower for the NASA 6% model than for the HARV.

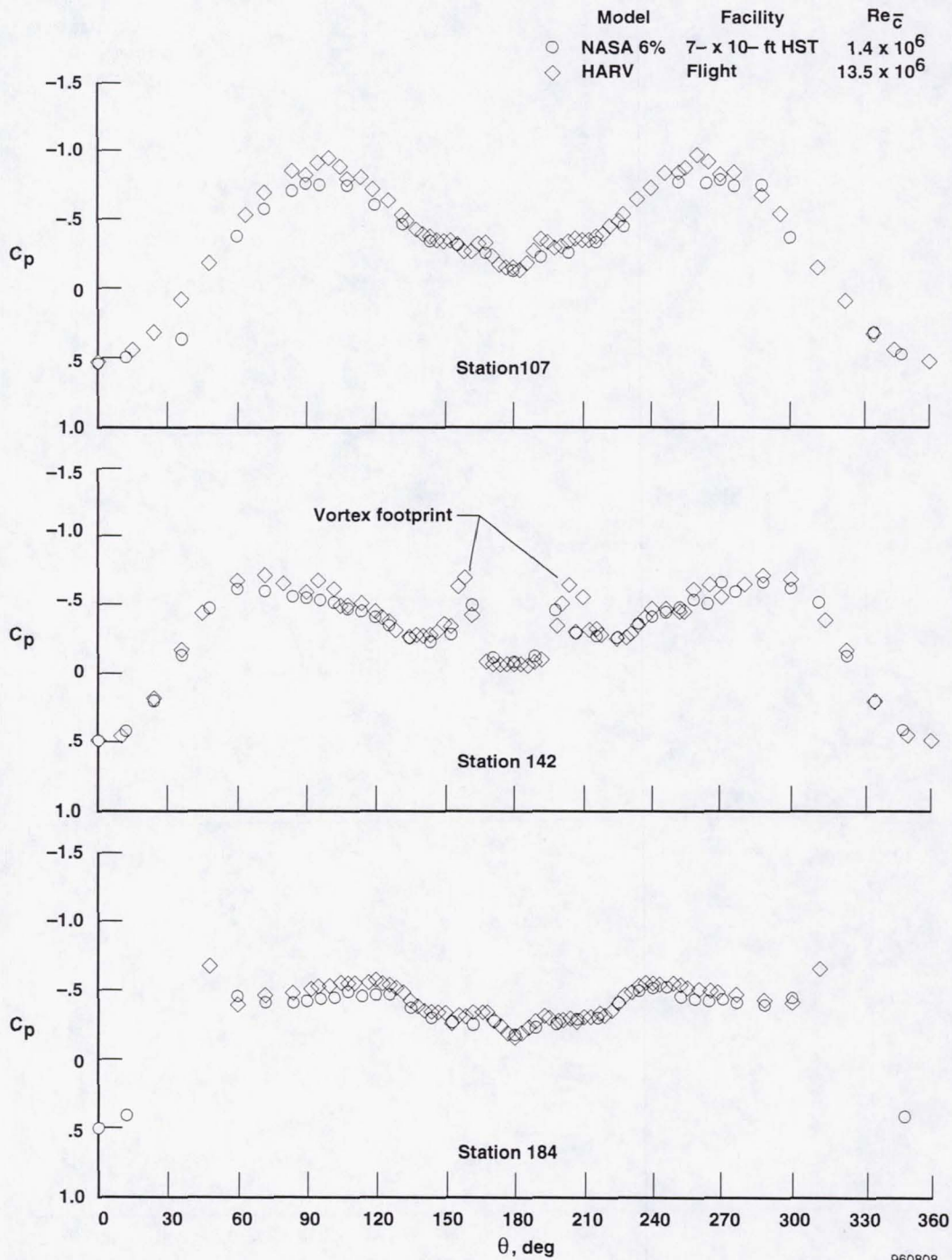


Figure 19. Comparison of forebody pressure distribution of NASA 6% F/A-18 model with fixed transition (twin strips no. 180 grit) to HARV. $\alpha = 40^\circ$, $M_\infty = 0.3$.

Figure 20 shows the effect of fixed forebody cross-flow transition on the lateral-directional stability of the NASA 6% model at $\alpha = 36.4^\circ$ and $M_\infty = 0.30$, with both 33° (fig. 20(a)) and 25° (fig. 20(b)) leading-edge flaps. Figure 21 shows the effects of fixed transition on the NASA-2 16% model at $\alpha = 40^\circ$ and $M_\infty = 0.08$, with both 33° (fig. 21(a)) and 25° (fig. 21(b)) leading-edge flaps. At these conditions the predominant effect of the fixed forebody transition is to increase lateral stability ($-4^\circ < \beta < 4^\circ$). The direct effect of fixing crossflow transition is to increase the strength of the forebody vortices at high angles of attack. This indicates that, at least for the F/A-18, fixing transition in sub-scale tests has a favorable effect on the lateral stability when there is an interaction of the forebody vortices and the LEX flow field. This effect is more pronounced with the 25° leading-edge flap deflection than with the 34° deflection, probably because of the more separated and presumably weaker wing flow field with the 25° leading-edge flap deflection. In other words, with the 34° leading-edge flaps deflection the wing flow is much more attached and stronger and therefore more likely to resist the influence from the LEX vortices. The lateral stability changes with leading-edge flap deflection were much more pronounced with the NASA

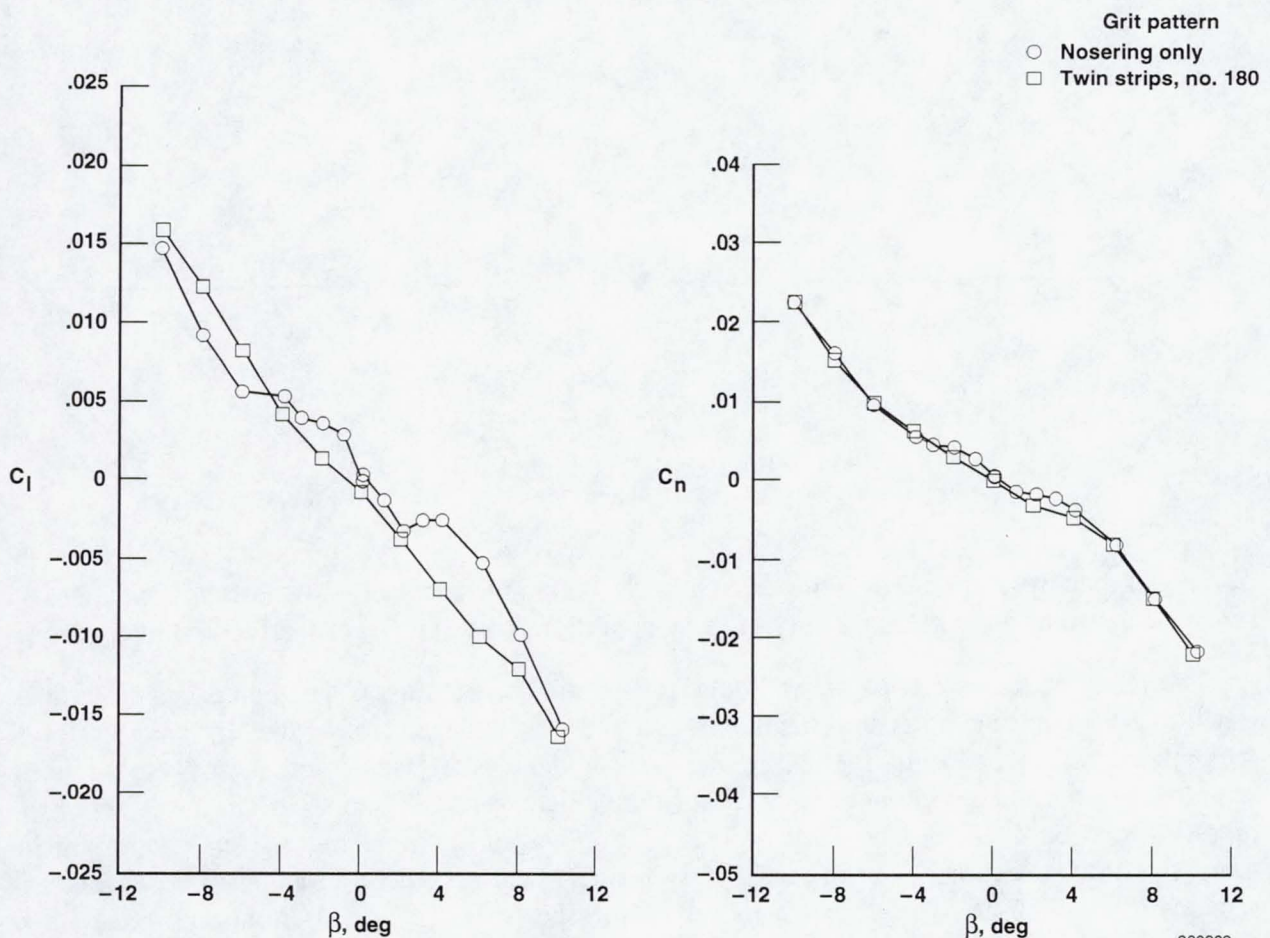
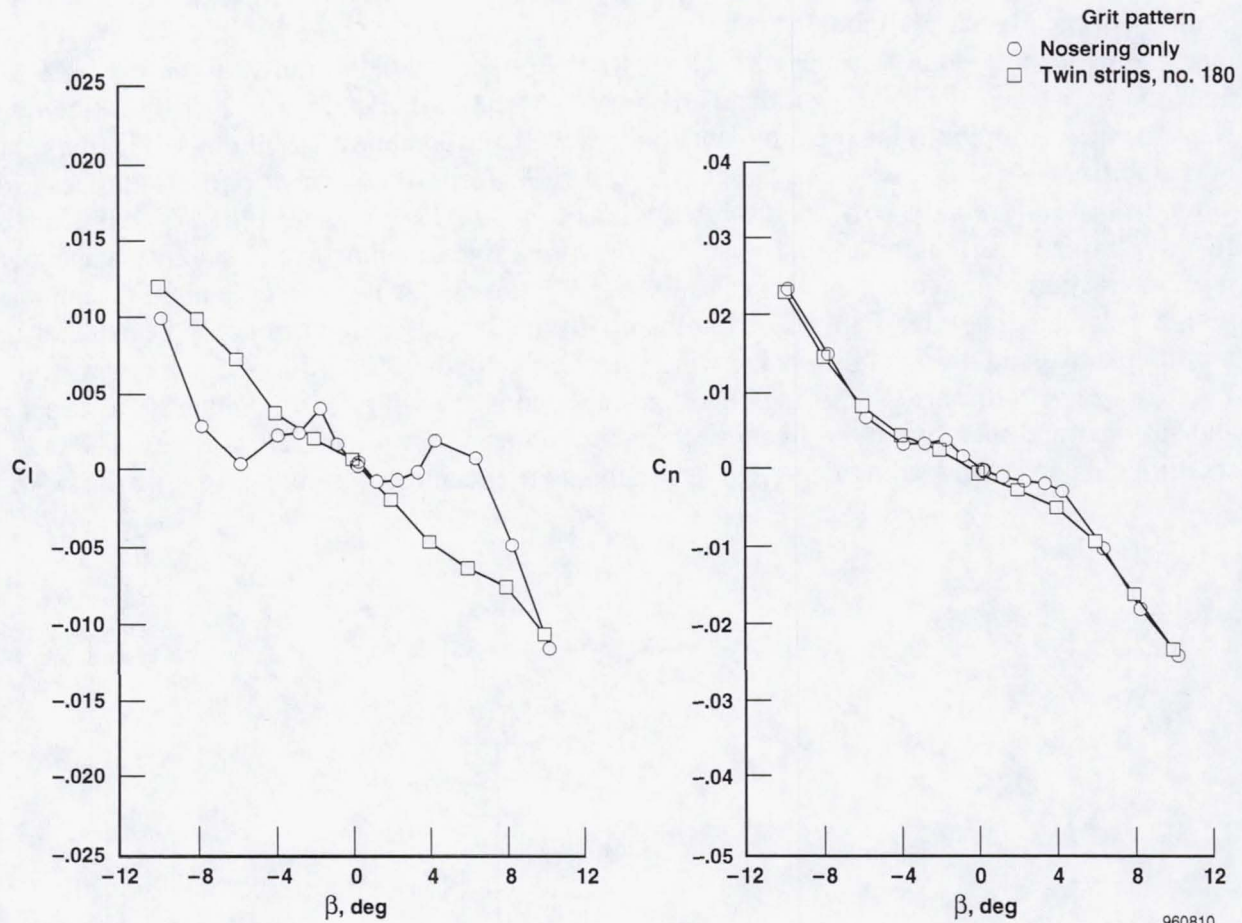


Figure 20. Effect of transition on lateral-directional stability of NASA 6% F/A-18 model. $\alpha = 36.4^\circ$, $M_\infty = 0.3$, $Re_{\bar{c}} \sim 1.4 \times 10^6$.

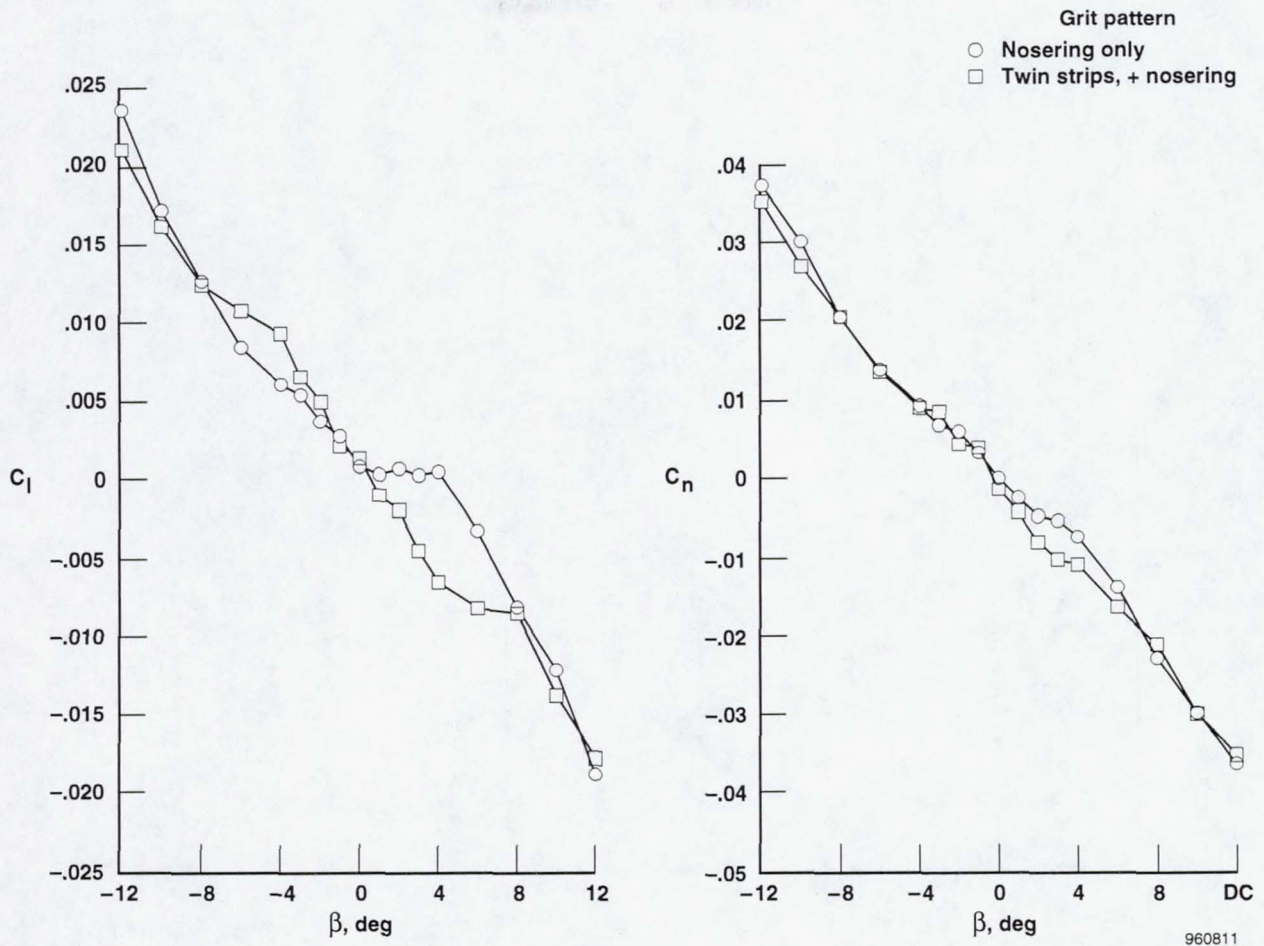


(b) $\delta_{LE} = 25^\circ$.

Figure 20. Concluded.

6% model than the NASA-2 16% model. This effect from the forebody flow field is dependent on several conditions and changes in any of these conditions can significantly effect the interaction.

The effect of pressure ports on a model can be similar to grit, that is they can cause the flow to transition. Whether the ports significantly disturb the flow is dependent on the size and density of the ports as well as the location. The NASA-2 16% model was fabricated with removable forebody sections both with and without pressure ports which made it possible to ascertain the effect of the pressure ports on the forebody. The forebody section was of the most interest, since variations in transition on this section has been seen as a significant factor on the high-angle-of-attack characteristics of the F/A-18. The effect of these pressure ports on the lateral-directional behavior is shown in figure 22. The effect of the pressure ports was very similar to that of gritting the forebody, such as shown in figure 21. The ports acted to transition the flow, similar to gritting, which strengthens the forebody vortices and subsequently increases lateral stability.

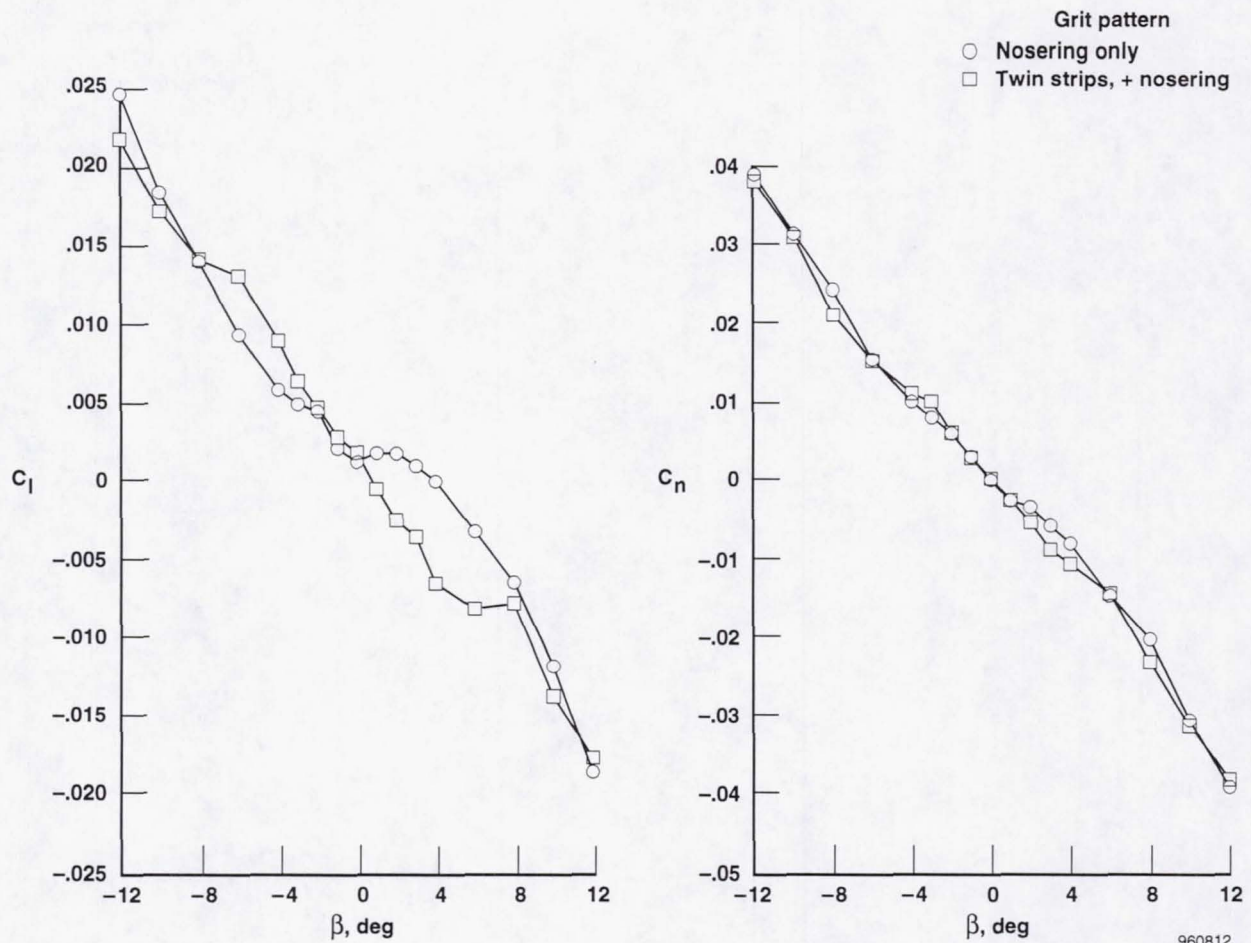


(a) $\delta_{fLE} = 33^\circ$.

Figure 21. Effect of transition on lateral-directional stability of NASA-2 16% F/A-18 model. $\alpha = 40^\circ$, $M_\infty = 0.08$, $Re_{\bar{c}} \sim 1 \times 10^6$.

Geometry Effects

Geometry effects are an obvious area of concern for correlation between models and model to flight. Small geometry changes that have minimal impact at low angles of attack can have large and pronounced effects at high angles of attack. For sharp and high fineness ratio forebodies at high angles of attack, even small variations at the nose can change the vortex shedding and the subsequent flow field.²⁷ The ramifications for high-angle-of-attack testing is that geometric fidelity in the forebody region warrants serious attention. The conventional sensitivities for low/moderate angle-of-attack testing must still be taken into consideration.



(b) $\delta_{fLE} = 25^\circ$.

Figure 21. Concluded.

Aft End Geometry Effects

Subtle geometry differences other than those at the forebody can also have a significant impact on high-angle-of-attack characteristics. The MD/Navy 6% scale model was designed to be tested at high dynamic pressures, and as such required a support sting capable of supporting the large loads, especially normal force and pitching moment. The support sting was large and elongated in the vertical axis so the model aft end had to be flared (distorted) to allow sufficient clearance from the sting (fig. 23, both the MD/Navy and NASA 6% models had a common aft end). Although this slight flaring of the aft end would appear to have minimal consequences it was suspected for being partly responsible for the significant pitching moment differences between the 6% and 16% models (fig. 7). At the higher angles of attack the NASA 6% model shows higher levels of nose down pitching moment than the NASA-2 16% model at $\alpha > 10^\circ$, even when the NASA 6% model was tested

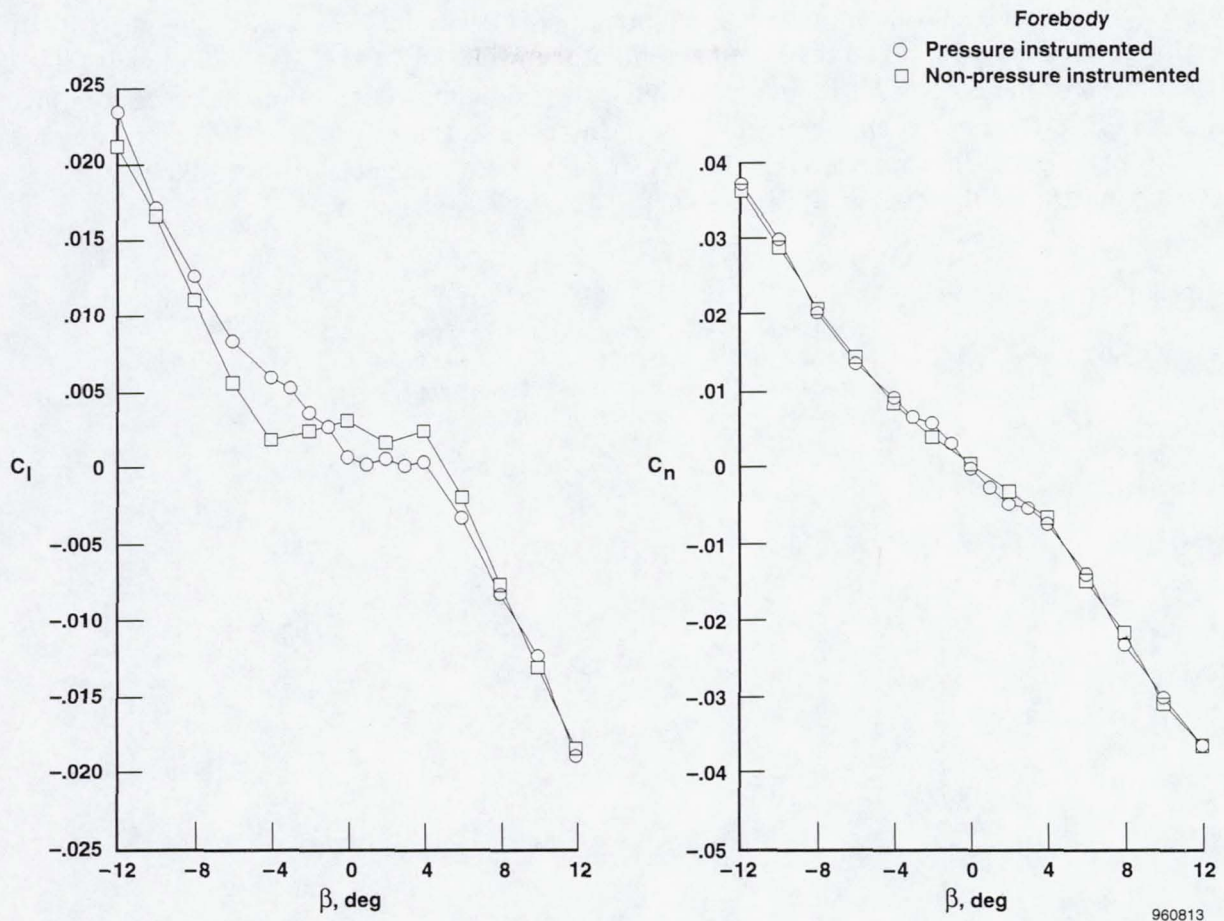


Figure 22. Effect of pressure ports on lateral-directional aerodynamics of NASA-2 16% F/A-18 model in the NASA Langley 30- x 60-ft Tunnel. $\alpha = 40^\circ$, $M_\infty = 0.08$, $\delta_{jLE} = 33^\circ$, $Re_{\bar{c}} \sim 1 \times 10^6$.

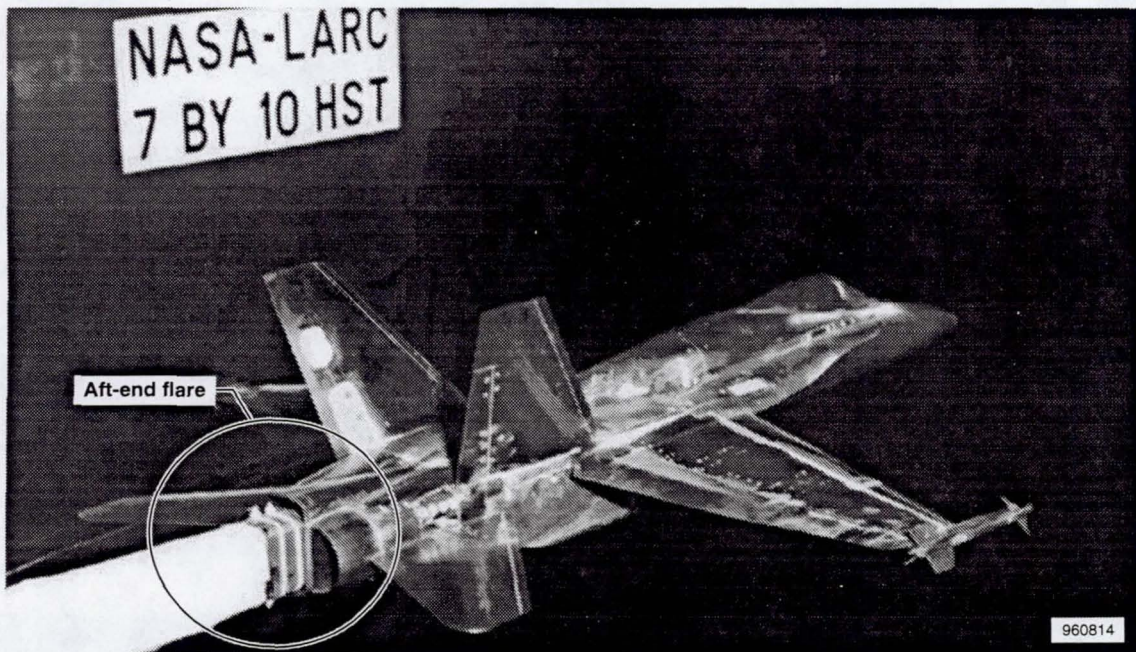


Figure 23. Photograph of NASA 6% F/A-18 model showing aft end flare.

at similar Reynolds or Mach numbers. A test was conducted of the NASA-2 16% model with pieces added to roughly represent the flared aft end of the MD/Navy and NASA 6% models (fig. 23). The results of the NASA-2 16% model with the flare simulated (fig. 24) made up approximately half the difference in pitching moment at high angles of attack ($25^\circ < \alpha < 45^\circ$) compared to the NASA 6% model. This indicates that the change in the back end geometry was likely responsible, at least in part, for this change in the high-angle-of-attack pitch behavior.

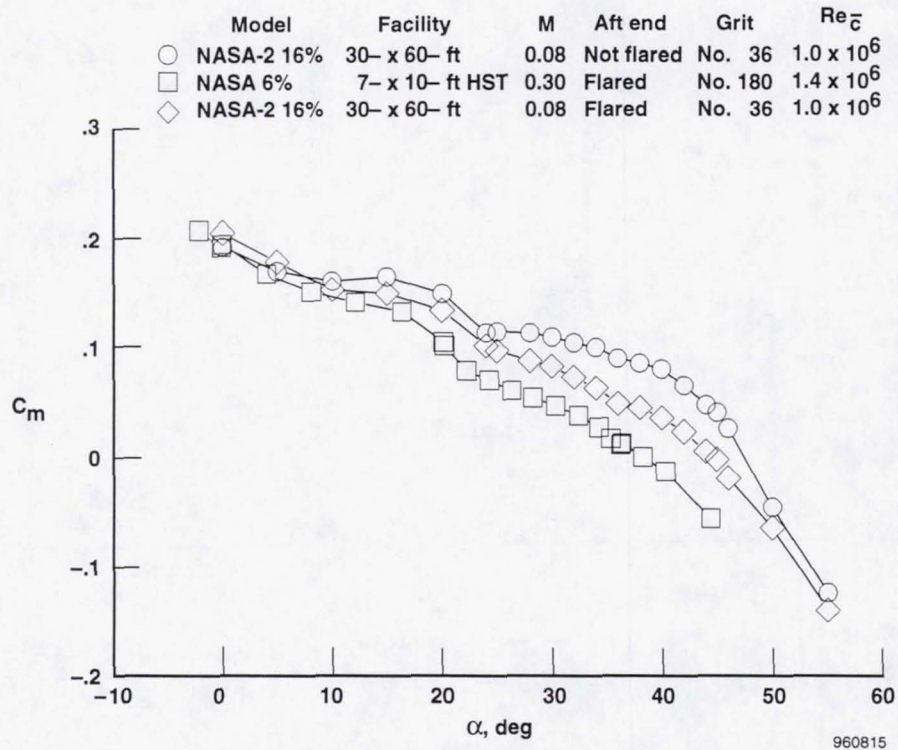


Figure 24. Effect of aft end flare on pitching moment of F/A-18 models. $\beta = 0^\circ$, $\delta_{fLE} = 33^\circ$, $\delta_{fTE} = 0^\circ$, $\delta_{HT} = -12^\circ$, twin strips.

Symmetric Forebody Strakes

Controlling separation on the forebody has been investigated for use as a yaw control device at high angles of attack.²⁸⁻³¹ During one such investigation of the effectiveness of deployable forebody strakes on the forebody of the NASA-2 16% model, symmetric deployments of the forebody strakes were tested. Figure 25 shows the results of symmetric strake deflections up to 30° . Increasing symmetric deflections of the forebody strakes at the deflection angles shown, increases lateral stability at angles of attack from approximately 30° to 50° . This is most likely caused by the increasing strength of the forebody vortices and favorable interaction with the LEX vortices. The effect is most pronounced near $\alpha = 40^\circ$, the angle of attack of maximum lift, which is where the disparity in lateral stability between the models was greatest.

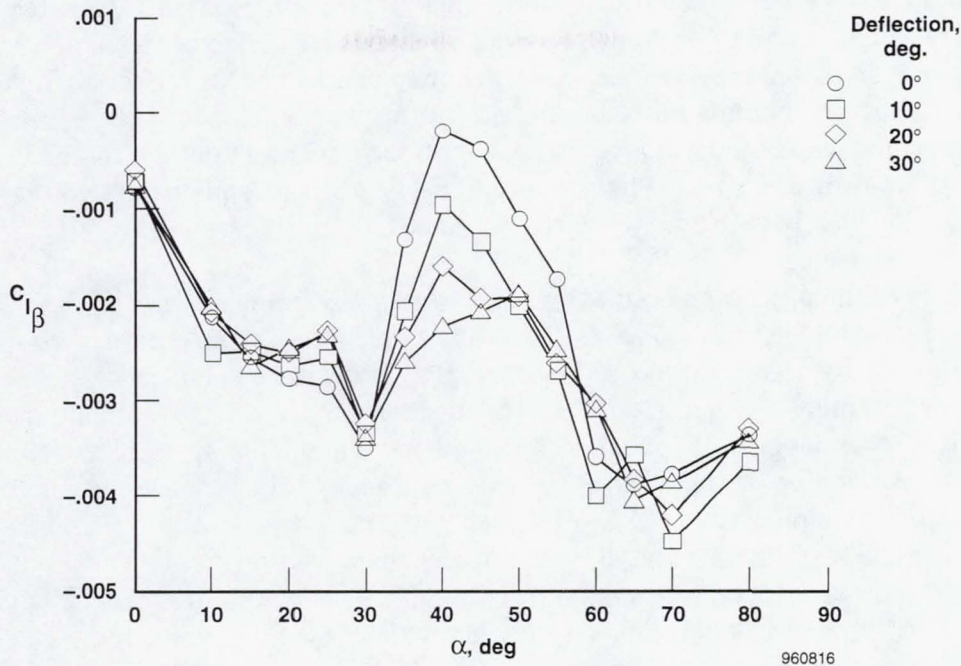


Figure 25. Effect of symmetric forebody strake deflections on lateral stability of the NASA-2 16% F/A-18 model. $M_\infty = 0.08$, $\delta_{fLE} = 33^\circ$, $\delta_{fTE} = 0^\circ$, $\Delta\beta = \pm 4^\circ$, $Re_{\bar{c}} \sim 1 \times 10^6$.

Noseboom Effects

The effect of adding a noseboom on a configuration can be extremely significant. Subtle changes in the geometry near the tip of a sharp or high fineness ratio forebody, at high angles of attack, can have a dramatic effect on the separation about that forebody, and subsequently the forebody flow (vortices) and downstream interactions. The noseboom has the combined effect of changing the tip geometry, increasing the effective fineness ratio, and propagating its own wake. This effect can be seen in the laser vapor screen off-surface flow visualization shown in figure 26. This was

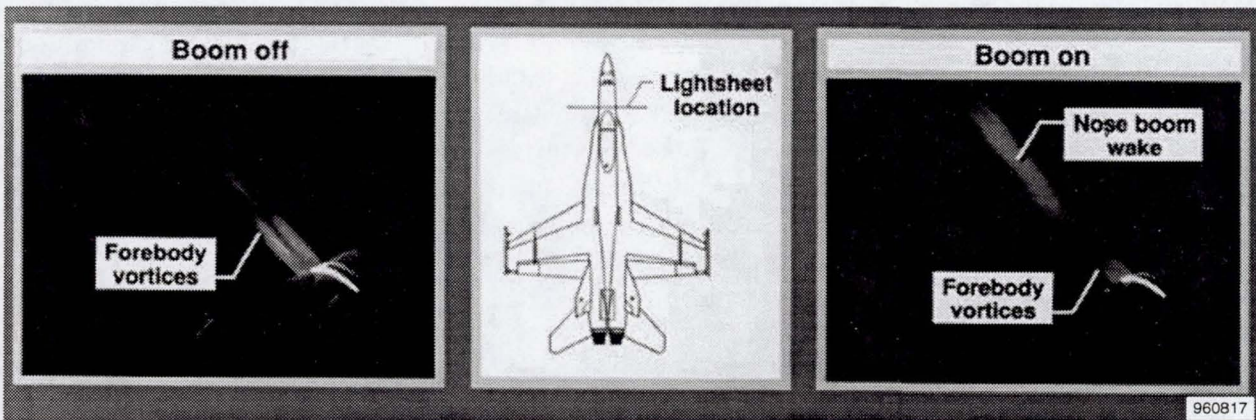


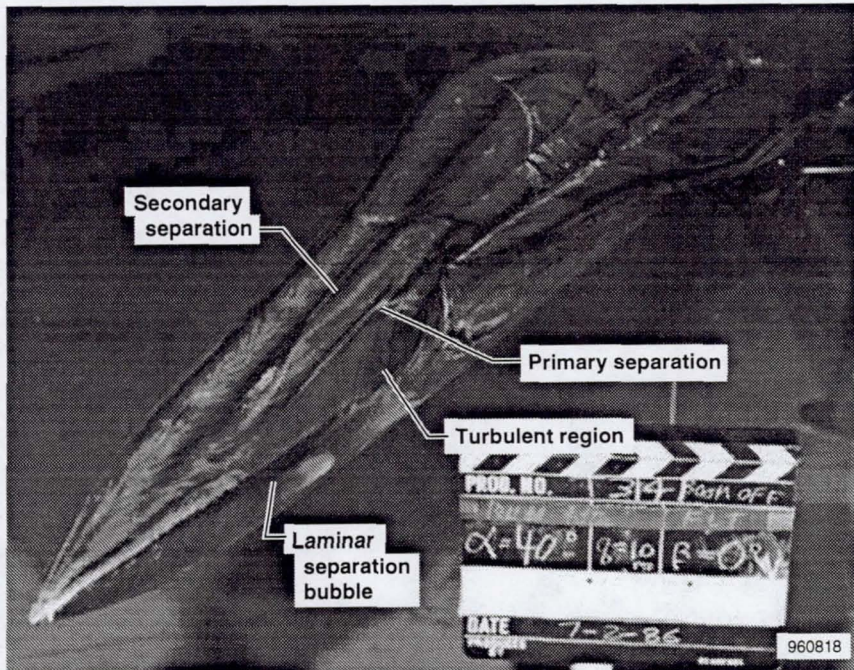
Figure 26. Flow visualization of NASA 6% F/A-18 forebody with and without noseboom. $\alpha = 50^\circ$, $\beta = 0^\circ$, $M_\infty = 0.6$, FS = 184. $Re_{\bar{c}} \sim 1.3 \times 10^6$.

obtained with the NASA 6% model at $M_\infty = 0.6$ and $\alpha = 50^\circ$, at the David Taylor Research Center 7- \times 10-ft Transonic Tunnel.²⁵ Although this was obtained at an angle of attack and Mach number greater than that discussed previously, it clearly shows the effect of the noseboom on the forebody flow field. Without the boom a fairly symmetric pair of well developed vortices can be observed at a station just forward of the canopy junction. With the noseboom on, the forebody vortices are significantly diminished in size, no longer appear as two separate and distinct vortices, and a significant wake can clearly be seen, presumably generated by the boom itself.

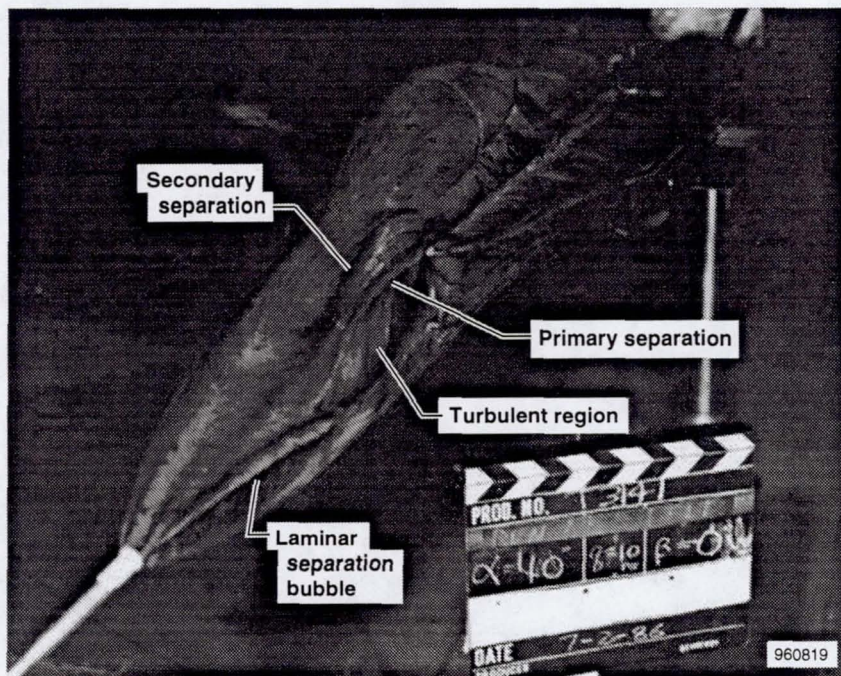
The effects of the noseboom on the forebody surface streamlines of the NASA-1 16% model at $\alpha = 40^\circ$ are shown in figure 27. Figure 27(a) shows the forebody surface flow without the noseboom and figure 27(b) shows the forebody surface flow at the same conditions with the noseboom. As would be expected with forebody vortices being attenuated, the surface streamlines are significantly softened when compared to those of the forebody without the boom. There are also weaker secondary separation lines that do not persist over the canopy. Figure 28 shows the forebody surface pressure distribution of the NASA 6% model with and without the noseboom at $\alpha = 37^\circ$ and $M_\infty = 0.3$. The major effect of the noseboom is to reduce the suction pressure peaks at FS 142, and show an indication of reduced forebody vortex strength. The lateral-directional characteristics of the NASA-2 16% and NASA 6% models with and without the noseboom, at $\alpha = 40^\circ$, are shown in figures 29 and 30, respectively. However, even though the effect of the boom on the forebody flow field is similar (reduced forebody vortex strength) between the two scale models, there is less of a sensitivity from the boom on the lateral-directional behavior of the NASA-2 16% than the NASA 6% with $\delta_{fLE} = 33^\circ$.

Leading-Edge Flap Effects

Leading-edge flaps can have a significant influence in this forebody/LEX flow interaction and therefore high-angle-of-attack lateral-directional stability. By reducing wing separation at a given angle of attack, leading-edge flaps can reduce the effects of the upstream flow field (i.e. the forebody and LEX flow fields). In the case of F/A-18 development, the lateral instability that was observed in the $C_{L,max}$ region was alleviated by increasing the leading-edge flap deflection from 25° to 33° . The effect of the leading-edge flap deflection and noseboom on lateral-directional stability of the two models is shown in figure 29 for the NASA-2 16% ($\alpha = 40^\circ$) model and figure 30 for the NASA 6% model ($\alpha = 37^\circ$). In both cases the destabilizing effect of the boom was reduced by increasing the leading-edge flap deflection. As seen previously the effect was more pronounced on the NASA 6% model than on the NASA-2 16%. This delayed wing flow separation to a higher angle of attack, and lessened the unstable effects of the LEX vortices acting on the mostly separated flow over the wing surfaces. Since the forebody vortices interact favorably with the LEX and the noseboom disrupts the forebody flow field and attenuates the forebody vortices, the noseboom is a destabilizing influence. However, with the leading-edge flap deflection increased to 33° this destabilizing influence is mitigated as shown in figure 30(b). The NASA-2 16% model showed much less sensitivity in lateral aerodynamics from this change in flap deflection.



(a) Noseboom off.



(b) Noseboom on.

Figure 27. Forebody flow visualization of NASA-2 16% F/A-18 model with and without noseboom. $\alpha = 40^\circ$, $\beta = 0^\circ$, $M_\infty = 0.08$, $Re_{\bar{c}} \sim 1 \times 10^6$.

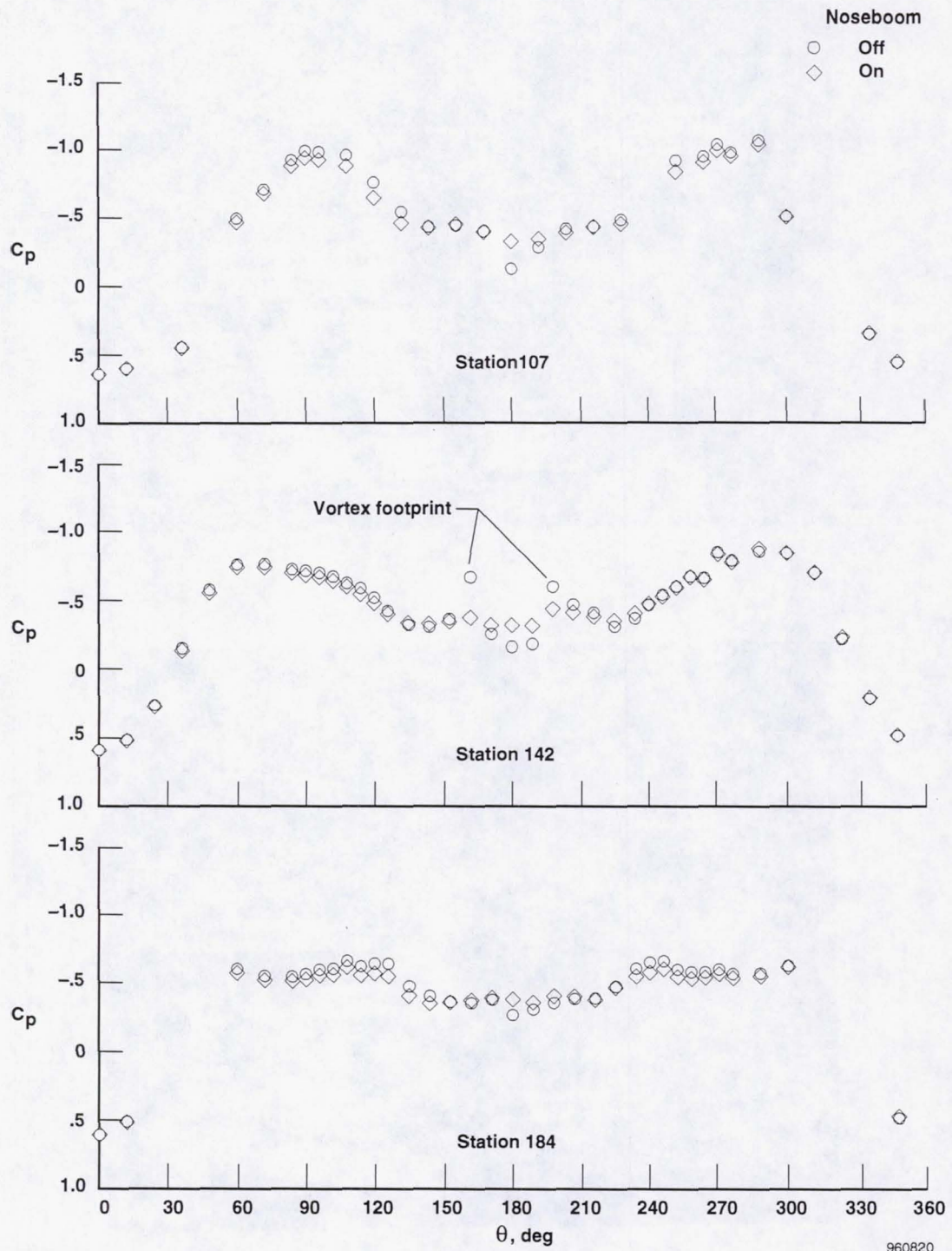
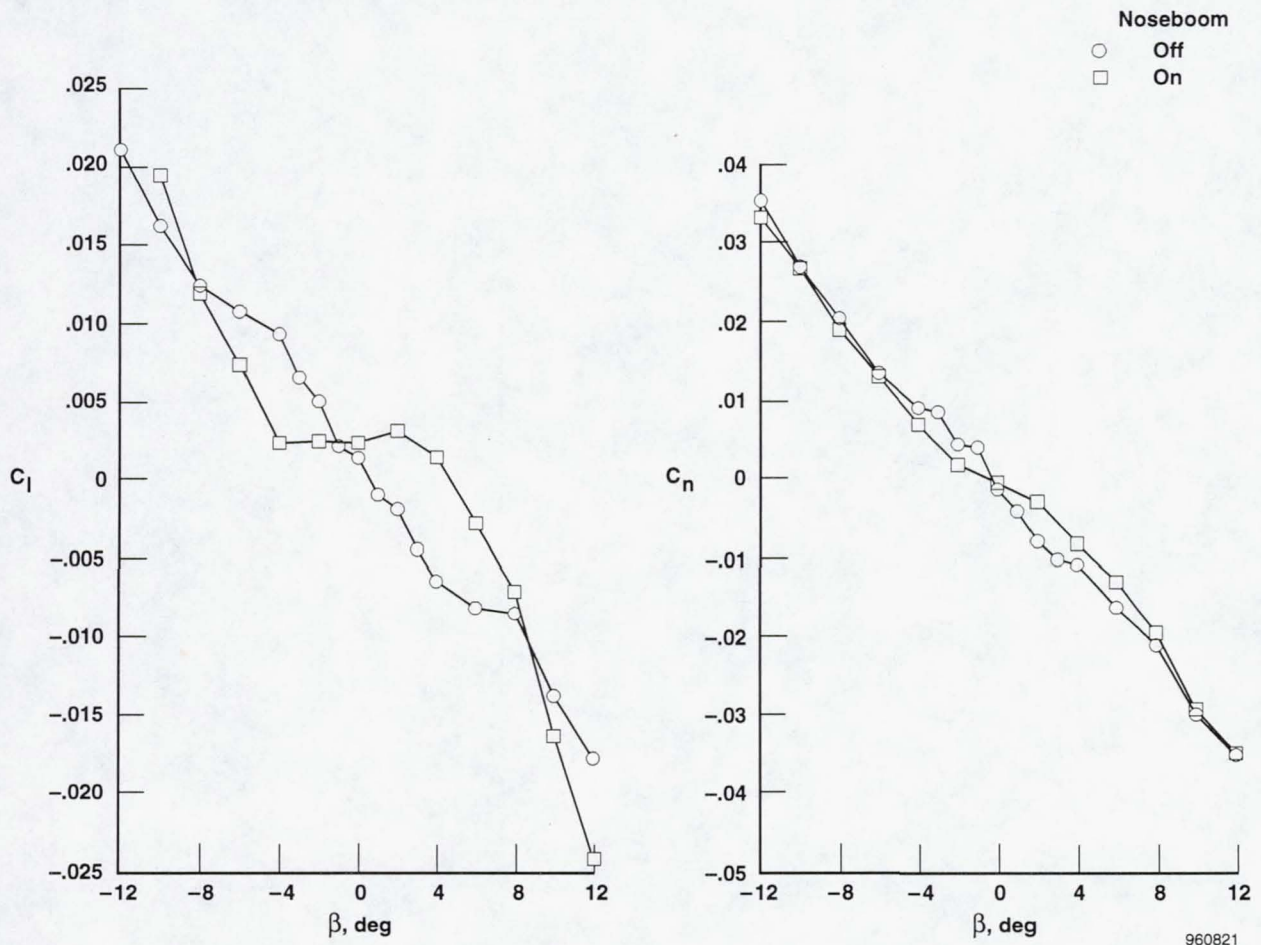
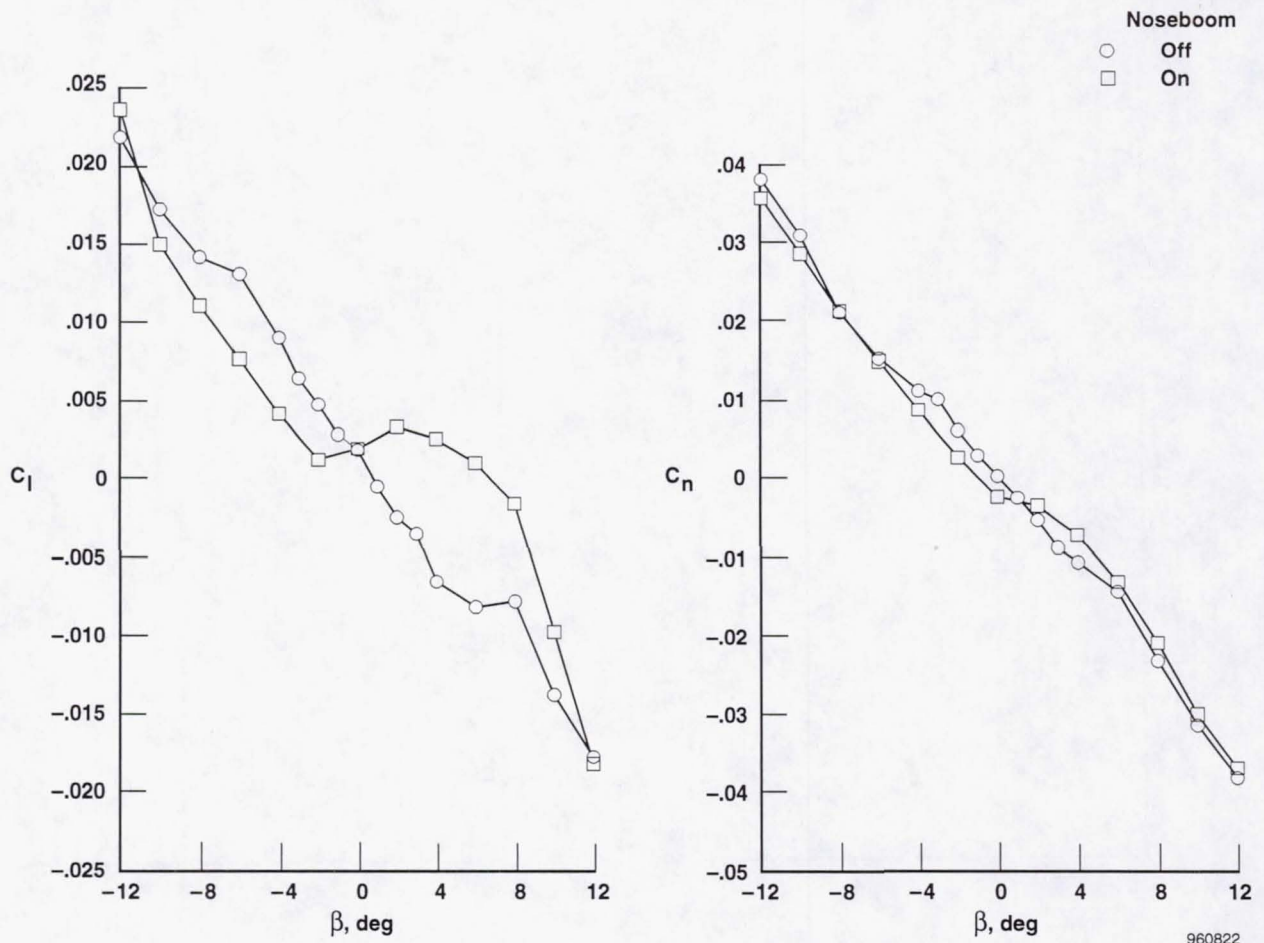


Figure 28. Effect of nose boom on forebody surface pressure distribution of NASA 6% F/A-18 model. $\alpha = 37^\circ$, $\beta = 0^\circ$, $M_\infty = 0.3$, $Re_{\bar{c}} \sim 1.4 \times 10^6$, twin strips no. 180 grit.



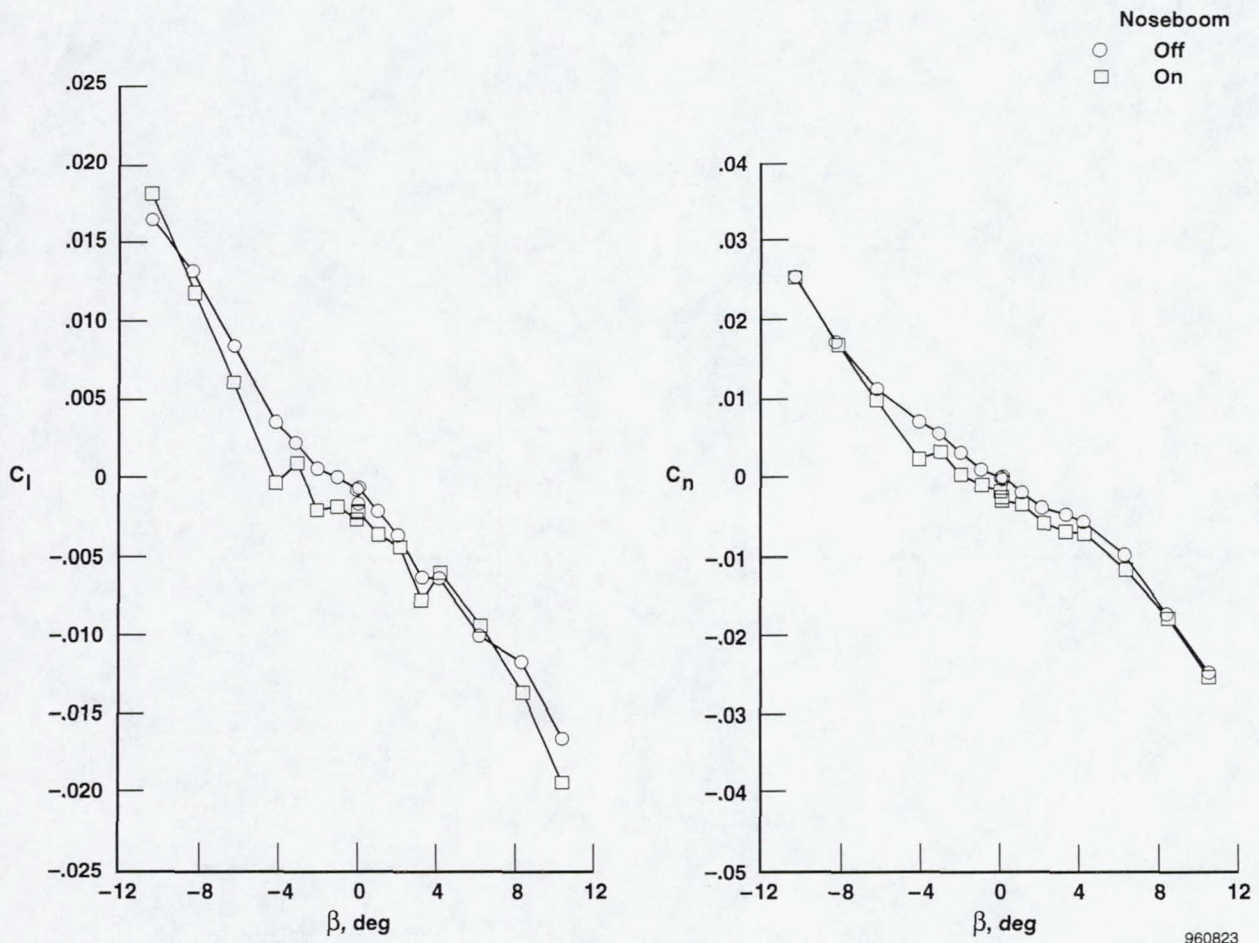
(a) $\delta_{fLE} = 33^\circ$.

Figure 29. Effect of noseboom on lateral-directional aerodynamics of NASA-2 16% F/A-18 model. $\alpha = 40^\circ$, $\beta = 0^\circ$, $M_\infty = 0.08$, $Re_{\bar{c}} \sim 1 \times 10^6$, twin strips no. 36 grit.



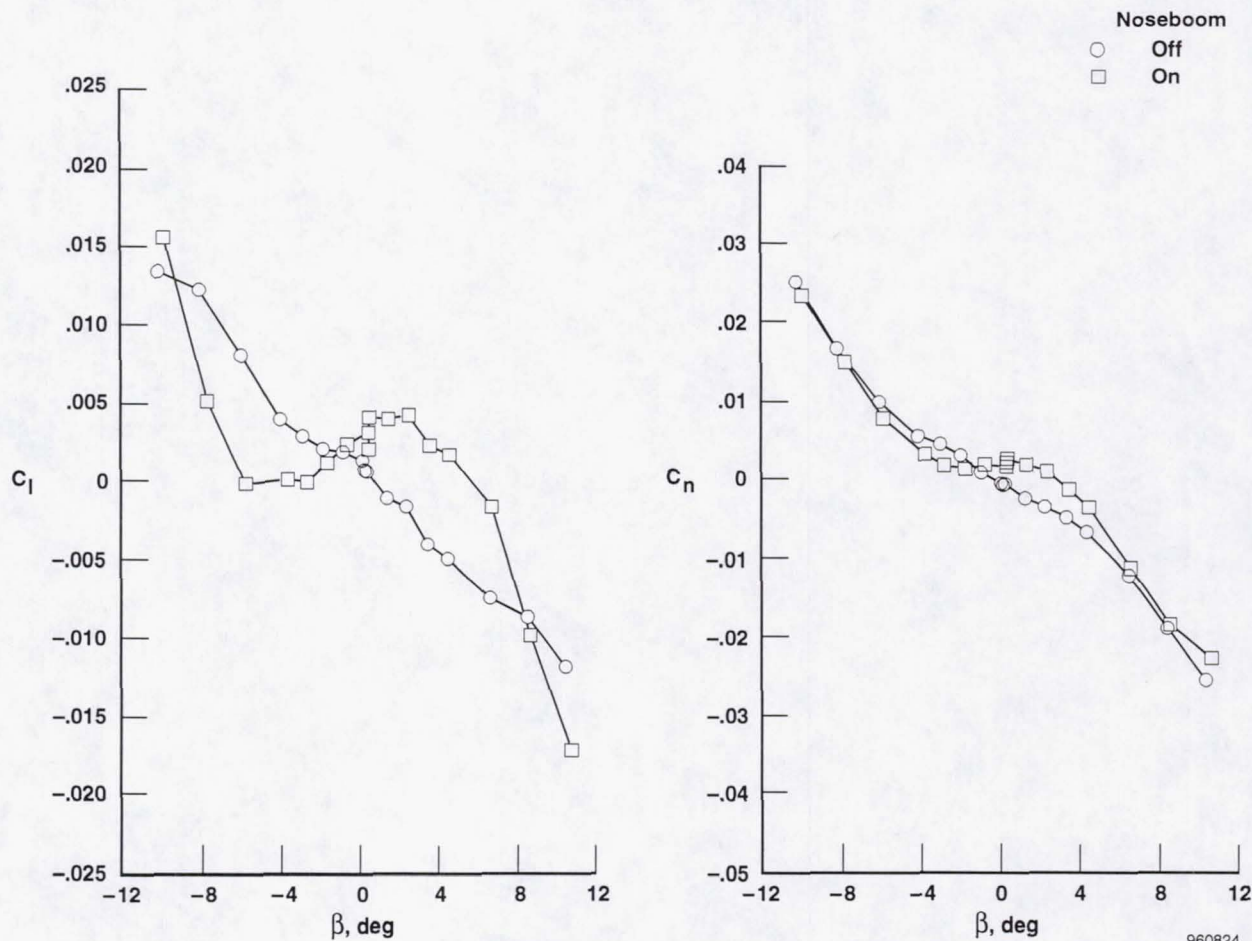
(b) $\delta_{fLE} = 25^\circ$.

Figure 29. Concluded.



(a) $\delta_{fLE} = 33^\circ$.

Figure 30. Effect of nose boom on lateral-directional aerodynamics of NASA 6% F/A-18 model. $\alpha = 37^\circ$, $\beta = 0^\circ$, $M_\infty = 0.3$, $Re_{\bar{c}} \sim 1.4 \times 10^6$, twin strips no. 180 grit.



(b) $\delta_{fLE} = 25^\circ$.

Figure 30. Concluded.

CONCLUDING REMARKS

A series of ground based and flight investigations have been conducted on the F/A-18 configuration as part of the NASA High-Angle-of-Attack Technology Program. One of the objectives of these investigations was to determine the causes of disparities between ground and flight results. The results indicate that crossflow on the forebody, leading-edge extension (LEX) flow fields, nosebooms, and aft distortions can have a paramount effect on ground-to-flight correlation at high angles of attack.

The differences seen in various sub-scale model tests at high angles of attack are due in part to the differences in forebody flow field and its subsequent interactions with the LEX and downstream flow fields. The forebody flow field is most sensitive to Reynolds number which drives its boundary layer state, and becomes increasingly important at high angles of attack. However, the LEX flow field is most sensitive to Mach number. It is difficult to match both conditions simultaneously during ground tests. Therefore, significant interactions at full-scale flight conditions may not be accurately predicted.

Fixing transition can simulate higher forebody Reynolds numbers, and therefore provide better predictions of full-scale flight results from sub-scale wind tunnel tests. At high angles of attack it is necessary to fix crossflow transition on the forebody in addition to conventional transition fixing for lower angles of attack. The twin strip technique has been shown to be effective on the F/A-18 configuration.

Pressure ports and other subtle configuration differences can have a significant effect on the forebody flow field, and on the overall configuration flow field. The effect of pressure ports is to add roughness similar to grit. These are more apparent at high angles of attack where the forebody flow field becomes more significant.

Geometric differences can often have pronounced effects at high angles of attack. Aft end distortions, due to wind tunnel support, on some F/A-18 models resulted in increased nose down pitching moments compared to the undistorted geometry. Symmetric forebody strakes can have a significant effect on the forebody vortices and increase lateral stability of the F/A-18 at angles of attack near that of maximum lift. Nose probes or other protuberances on the forebody, especially near the tip, have a significant influence on the forebody flow field. These influences can reduce forebody vortex strength at high angles of attack and cause a reduction in lateral stability on the F/A-18. Increasing leading-edge flap deflection at high angles of attack decreases wing flow separation and reduces the effects of upstream influences; that is the LEX and forebody vortex flows in the case of the F/A-18. The combined effect of the nose probe and reduced leading-edge flap deflection can result in lateral instability at angles of attack near maximum lift for the F/A-18.

REFERENCES

¹Gilbert, William P. and Gatlin, Donald H., "Review of the NASA High-Alpha Technology Program," *High-Angle-of-Attack Technology Conference*, NASA CR-3149, pt. 1, vol. 1, Oct. 30–Nov. 1, 1992, pp. 23–59.

²Lee, B.H.K., Brown, D., Zgela, M., and Poirer, D., "Wind Tunnel Investigation and Flight Tests of Tail Buffet on the CF-18 Aircraft," *AGARD Specialists' Meeting on Aircraft Loads due to Flow Separation*, Sorrento, Italy, Apr. 1–6, 1990.

³Meyn, L.A. and James, K.D., "Full-Scale Wind Tunnel Studies of F/A-18 Tail Buffet," AIAA-93-3519, Monterey, CA, 1993.

⁴Meyn, L.A., James, K.D., and Geenen, R.J., *Correlation of F/A-18 Tail Buffet Results*, NASA CP 10143, Fourth High Alpha Conference, NASA Dryden Flight Research Center, Edwards, CA, July 12–14, 1994.

⁵Shah, Gautam H., Grafton, Sue B., Guynn, Mark D., Brandon, Jay M., Dansberry, Bryan E., and Patel, Suresh R., "Effect of Vortex Flow Characteristics on Tail Buffet and High-Angle-of-Attack Aerodynamics of a Twin-Tail Fighter Configuration," presented at *NASA High-Angle-of-Attack Technology Conference*, NASA Langley Research Center, Hampton, Virginia, Oct. 30–Nov. 1, 1990.

⁶Shah, Gautam H., "Wind Tunnel Investigation of Aerodynamic and Tail Buffet Characteristics of Leading-Edge Extension Modifications to the F/A-18," AIAA-91-2889. Presented at *AIAA Atmospheric Flight Mechanics Conference*, New Orleans, LA, Aug., 1991.

⁷Quast, Thomas, Nelson, Robert C., and Fisher, David F., *A Study of High Alpha Dynamics and Flow Visualization for a 2.5-percent Model of the F-18 HARV Undergoing Wing Rock*, AIAA-91-3267, Jan. 1991.

⁸Fisher, David F., DelFrate, John H., and Richwine, David M., *In-Flight Flow Visualization Characteristics of the NASA F-18 High Alpha Research Vehicle at High Angles of Attack*, NASA TM-4193, May 1990.

⁹Erickson, Gary E., *Water Tunnel Flow Visualization and Wind Tunnel Data Analysis of the F/A-18*, NASA CR-165859, May 1982.

¹⁰Hall, R.M. and Banks, D.W., *Progress in Developing Gritting Techniques for High Angle of Attack Flows*, AIAA-94-0169, Jan. 1994.

¹¹Hall, R.M., Erickson, G.E., Banks, D.W., and Fisher, D.F., "Advances in High-Alpha Experimental Aerodynamics; Ground Test and Flight," *High-Angle-of-Attack Technology Conference*, Publication 3149, pt. 1, vol. 1, Oct. 30–Nov. 1, 1990, pp. 69–115.

¹²Banks, D.W., Fisher, D.F., Erickson, G.E., Jordan, F.L., Hall, R.M., and Sewall, W.G., "Comparison of Wind Tunnel and Flight Forebody Flow Fields on the NASA F-18 High-Alpha Research Vehicle," *High-Angle-of-Attack Technology Conference*, Publication 3149, pt. 1, vol. 1, Oct. 30–Nov. 1, 1992, pp. 243–264.

¹³Banks, Daniel W., Hall, Robert M., Erickson, Gary E., and Fisher, David F., *Forebody Flow Field Effects on the High Angle-of-Attack Lateral-Directional Aerodynamics of the F/A-18*, AIAA-94-0170, Jan. 1994.

¹⁴Banks, Daniel W., *Wind-Tunnel Investigation of the Forebody Aerodynamics of a Vortex-Lift Fighter Configuration at High Angles of Attack*, SAE-881419, Oct. 1988.

¹⁵Erickson, G.E., Hall, R.M., Banks, D.W., DelFrate, J.H., Schreiner, J.A., Hanley, R., and Pulley, C.T., *Experimental Investigation of the F/A-18 Vortex Flows at Subsonic Through Transonic Speeds*, AIAA-89-2222, Aug. 1989.

¹⁶Bowers, Albion H., Pahle, Joseph, Wilson, Joseph R., Flick, Bradley C., and Rood, Richard L., "An Overview of the NASA F-18 High Alpha Research Vehicle," *High-Angle-of-Attack Technology Conference*, Langley Research Center, Hampton, Virginia, Sept. 17–19, 1996.

¹⁷Schneider, Edward T. and Meyer, Robert R., Jr., "F-18 High Alpha Research Vehicle Description, Results, and Plans," *Society of Experimental Test Pilots, Thirty-Third Symposium Proceedings*, Sept. 1989, pp. 135–162.

¹⁸Fisher, David F., Banks, Daniel W., and Richwine, David M., *F-18 High Alpha Research Vehicle Surface Pressures: Initial In-Flight Results and Correlation with Flow Visualization and Wind Tunnel Data*, AIAA-90-3018, Aug. 1990.

¹⁹Fisher, David F., Richwine, David M., and Banks, Daniel W., *Surface Flow Visualization of Separated Flows on the Forebody of an F/A-18 Aircraft and Wind-Tunnel Model*, NASA TM-100426, also available as AIAA-88-2112, June 1988.

²⁰Curry, Robert E. and Richwine, David M., *An Airborne System for Vortex Flow Visualization on the F-18 High-Alpha Research Vehicle*, AIAA-88-4671-CP, Sept. 1988.

²¹Richwine, David M., Curry, Robert E., and Tracy, Gene V., *A Smoke Generator System for Aerodynamic Flight Research*, NASA TM-4137, Sept. 1989.

²²Lamont, P.J., *The Effect of Reynolds Number on Normal and Side Forces on Ogive-Cylinders at High Incidence*, AIAA-85-1799, Aug. 1985.

²³Keener, Earl R., *Flow-Separation Patterns on Symmetric Forebodies*, NASA TM-86016, Jan. 1986.

²⁴Hunt, B.L., *Asymmetric Vortex Forces and Wakes on Slender Bodies (Invited paper)*, AIAA-82-1336, Aug. 1982.

²⁵Erickson, Gary E., *Wind Tunnel Investigation of Vortex Flows on F/A-18 Configuration at Subsonic Through Transonic Speeds*, NASA TP-3111, Dec. 1991.

²⁶Braslow, A.L., Harris, R.V., Jr., and Hicks, R.M., *Use of Grit-Type Boundary-Layer Transition Trips on Wind-Tunnel Models*, NASA TN-D-3579, Sept. 1966.

²⁷Moskovitz, Cary A., DeJarnette, F.R., and Hall Robert M., *Effects of Nose Bluntness, Roughness, and Surface Perturbations on the Asymmetric Flow Past Slender Bodies at Large Angles of Attack*, AIAA-89-2236, Jan. 1989.

²⁸Murri, Daniel G., Biedron, Robert T., Erickson, Gary E., Jordan, Frank L., Jr., and Hoffer, Keith D., "Development of Actuated Forebody Strake Controls for the F-18 High Alpha Research Vehicle," NASA CP-3149, pp. 335–380. Presented at the *NASA High-Angle-of-Attack Technology Conference*, Hampton, Virginia, Oct 30–Nov. 1, 1990.

²⁹Erickson, Gary E., and Murri, Daniel G., "Forebody Strakes for High-Angle-of-Attack Vortex Flow Control - Mach Number and Strake Planform Effects," NASA CP-3149, pp. 381–480. Presented at the *NASA High-Angle-of-Attack Technology Conference*, Hampton, Virginia, Oct. 30–Nov. 1, 1990.

³⁰Murri, Daniel G., Shah, Gautam H., DiCarlo, Daniel J., and Trilling, Todd W., "Actuated Forebody Strake Controls for the F-18 High-Alpha Research Vehicle," *Journal of Aircraft*, vol. 32, no. 3, May–June 1995, pp. 555–562.

³¹Murri, Daniel G., Fisher, David F., and Lanser, Wendy R., "Effect of Actuated Forebody Strakes on the Forebody Aerodynamic of the NASA HARV," Presented at the *NASA High-Angle-of-Attack Technology Conference*, Hampton, Virginia, Sept. 17–19, 1996.

REPORT DOCUMENTATION PAGE

Form Approved
OMB No. 0704-0188

Public reporting burden for this collection of information is estimated to average 1 hour per response, including the time for reviewing instructions, searching existing data sources, gathering and maintaining the data needed, and completing and reviewing the collection of information. Send comments regarding this burden estimate or any other aspect of this collection of information, including suggestions for reducing this burden, to Washington Headquarters Services, Directorate for Information Operations and Reports, 1215 Jefferson Davis Highway, Suite 1204, Arlington, VA 22202-4302, and to the Office of Management and Budget, Paperwork Reduction Project (0704-0188), Washington, DC 20503.

1. AGENCY USE ONLY (Leave blank)		2. REPORT DATE January 1997	3. REPORT TYPE AND DATES COVERED Technical Memorandum	
4. TITLE AND SUBTITLE The F/A-18 High-Angle-of-Attack Ground-to-Flight Correlation: Lessons Learned			5. FUNDING NUMBERS WU 505-68-30	
6. AUTHOR(S) Daniel W. Banks, David F. Fisher, Robert M. Hall, Gary E. Erickson, Daniel G. Murri, Sue B. Grafton, and William G. Sewall				
7. PERFORMING ORGANIZATION NAME(S) AND ADDRESS(ES) NASA Dryden Flight Research Center P.O. Box 273 Edwards, California 93523-0273			8. PERFORMING ORGANIZATION REPORT NUMBER H-2149	
9. SPONSORING/MONITORING AGENCY NAME(S) AND ADDRESS(ES) National Aeronautics and Space Administration Washington, DC 20546-0001			10. SPONSORING/MONITORING AGENCY REPORT NUMBER NASA TM-4783	
11. SUPPLEMENTARY NOTES Presented at NASA Langley High-Angle-of-Attack Technology Conference, Langley Research Center, Hampton, Virginia, September 17-19, 1996. Daniel Banks and David Fisher, Dryden Flight Research Center, Edwards, CA; Robert Hall, Gary Erickson, Daniel Murri, Sue Grafton, and William Sewall, NASA Langley Research Center, Hampton, VA.				
12a. DISTRIBUTION/AVAILABILITY STATEMENT Unclassified—Unlimited Subject Category 02			12b. DISTRIBUTION CODE	
13. ABSTRACT (Maximum 200 words) Detailed wind tunnel and flight investigations were performed on the F/A-18 configuration to explore the causes of many high-angle-of-attack phenomena and resulting disparities between wind tunnel and flight results at these conditions. Obtaining accurate predictions of full-scale flight aerodynamics from wind-tunnel tests is important and becomes a challenge at high-angle-of-attack conditions where large areas of vortical flow interact. The F/A-18 airplane was one of the first high-performance aircraft to have an unrestricted angle-of-attack envelope, and as such the configuration displayed many unanticipated characteristics. Results indicate that fixing forebody crossflow transition on models can result in a more accurate match of flow fields, and thus a more accurate prediction of aerodynamic characteristics of flight at high angles of attack. The wind tunnel results show that small geometry differences, specifically nosebooms and aft-end distortion, can have a pronounced effect at high angles of attack and must be modeled in sub-scale tests in order to obtain accurate correlations with flight.				
14. SUBJECT TERMS Fighter aircraft; Forebody flows; High angle of attack; Vortex flows; Vortex interactions			15. NUMBER OF PAGES 43	
			16. PRICE CODE AO3	
17. SECURITY CLASSIFICATION OF REPORT Unclassified	18. SECURITY CLASSIFICATION OF THIS PAGE Unclassified	19. SECURITY CLASSIFICATION OF ABSTRACT Unclassified	20. LIMITATION OF ABSTRACT Unlimited	